Gondwana Research 22 (2012) 310–324

Contents lists available at SciVerse ScienceDirect

Gondwana Research

journal homepage: www.elsevier.com/locate/gr

Mineral chemistry, trace elements and Sr–Nd–Hf isotope geochemistry and petrogenesis of Cailing and Furong granites and mafic enclaves from the Qitianling batholith in the Shi-Hang zone, South China

Kui-Dong Zhao, Shao-Yong Jiang *, Shui-Yuan Yang, Bao-Zhang Dai, Jian-Jun Lu

State Key Laboratory for Mineral Deposits Research, School of Earth Sciences and Engineering, Nanjing University, Nanjing, 210093, PR China

ARTICLE INFO

Article history:
Received 17 January 2011
Received in revised form 26 September 2011
Accepted 28 September 2011
Available online 13 October 2011

Handling Editor: Z. Zhang

Keywords:
A-type granite
Mafic microgranular enclaves (MMEs)
Zircon Hf isotope
Shi-Hang zone
South China

ABSTRACT

The Shi-Hang zone is an important NE trending Mesozoic magmatic belt composed of granites with relative high $\varepsilon_{Nd}(t)$ values and young T_{DM} model ages in South China. However, the petrogenesis and the tectonic environment for the Shi-Hang zone magmatic rocks remain controversial. We report here mineral chemistry, geochemical and Sr–Nd–Hf isotopic data for the Cailing and Furong granites and mafic microgranular enclaves (MMEs) from the Qitianling granite batholith in southern Hunan province, South China. The Qitianling granite batholith is a multi-staged composite pluton with three phases (Cailing, Furong, and Huangtangling) according to their ages and petrography. The Cailing (163–160 Ma) and Furong (157–153 Ma) phases are mainly composed of porphyritic amphibole–biotite monzogranite, and they share similar geochemical and isotopic characteristics. Both of them show similar SiO_2 contents from 66.50 to 70.28%, and metaluminous A/CNK values of 0.80 to 0.98. The granites are characterized by high contents of large ion lithosphile elements (LILE) such as Rb, Th, U, Pb; high field strength elements (HFSE) such as Nb, Ta, Zr, Hf; and Zr + Nb + Ce + Y contents > 350 ppm, and high 10,000 * Ga/Al ratios > 2.6. Chondrite-normalized REE patterns show relative enrichment of light rare earth elements (LREEs) and significant negative Eu anomalies. Mineralogical and geochemical features suggest that the Cailing and Furong granites are A-type, which can be further classified as A_2 subtype. They have relatively lower $(^{87}Sr/^{86}Sr)_i$ ratios (0.7091–0.7132), higher $\varepsilon_{Nd}(t)$ values (−5.5 to −7.6) and younger Nd isotopic model ages (1.48–1.56 Ga) than those common S-type granites in South China. Zircon $\varepsilon_{Hf}(t)$ values vary from −8.1 to −3.7. The MMEs in the Cailing phase show similar trace element and Sr–Nd isotopic characteristics with the host granites. But zircons from the MMEs show different $\varepsilon_{Hf}(t)$ values (−6.4–+2.6) with those from the host granites (−8.1 to −3.7). This indicates that the MMEs and host granites were crystallized from different sources of magmas, providing direct evidence for mafic–felsic magma mixing processes. The isotope data indicate that the Cailing and Furong granites from the Qitianling batholith were derived from a hybrid magma consisting of about 80% felsic magma derived from old crust and about 20% mantle-derived mafic magma. The strong magma mixing at about 160–155 Ma caused by intra-arc rifting or back arc extension related to subduction of the Paleo-Pacific plate, is favored to explain the petrogenesis of the Cailing and Furong granites, as well as the Shi-Hang zone.

1. Introduction

The Mesozoic geology of Southeastern China is characterized by widespread igneous rocks consisting predominantly of granite, rhyolite and subordinate mafic intrusive and volcanic rocks. These igneous rocks fall in three main age groups, the Triassic (commonly referred to as "Indosinian") intrusions, the Jurassic ("Early Yanshanian") and the Cretaceous ("Late Yanshanian") igneous rocks. Despite intensive scientific research, the geodynamic setting of these complexes remains controversial, especially for the early Yanshanian magmatism. Different models have been proposed in the last two decades, and the focal question is whether the magmatism was associated with the subduction of the Paleo-Pacific plate beneath the Eurasia plate (e.g. Zhou and Li, 2000; Jiang et al., 2005, 2006b; Zhou et al., 2006; Li and Li, 2007; Li et al., 2007b; Jiang et al., 2009; Zhou et al., 2011) or intraplate extension and/or continental rifting regime caused by collision between Indochina and South China during early Mesozoic times (e.g. Gilder et al., 1996; Wang et al., 2003c; Zhu et al., 2006a; Chen et al., 2008).

Previous studies have revealed a northeast-trending magmatic zone with relatively high ε_{Nd} (t) values and low T_{DM} values (the so-called Shi-Hang zone, Gilder et al., 1996) in the interior of South China Block. The zone was further to separate into the South belt and the North belt (Fig. 1a) (Chen and Jahn, 1998). These granites in

* Corresponding author.
E-mail address: shyjiang@nju.edu.cn (S.-Y. Jiang).

1342-937X/$ – see front matter
doi:10.1016/j.gr.2011.09.010

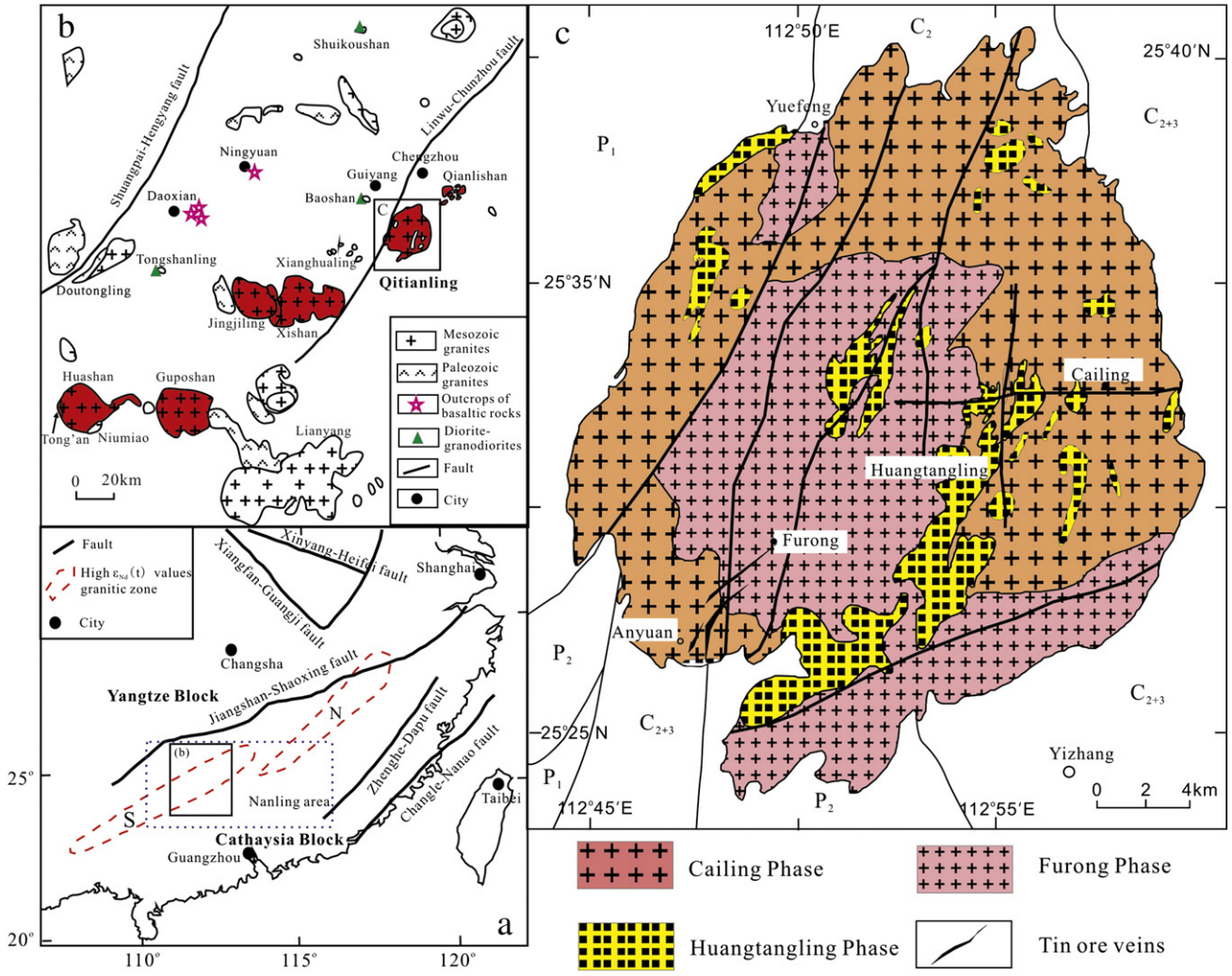

Fig. 1. (a) Sketch map showing the Shi-Hang zone in South China (N = the North belt, S = the South belt, modified from Chen and Jahn, 1998); (b) Simplified geological map of the southern Hunan and northern Guangxi region; (c) Simplified geological map of the Qitianling granites (modified from Zhu et al., 2009).

the Shi-Hang zone are characterized by significantly higher Sm (>8 ppm) and Nd (>45 ppm) with relatively higher $\varepsilon_{Nd}(t)$ values (−2 to −8) and younger T_{DM} ages (<1.5 Ga) (Gilder et al., 1996; Chen and Jahn, 1998). The Shi-Hang zone was interpreted as a result of mantle upwelling along a "paleo-rift" (Gilder et al., 1996). The southern Hunan and northern Guangxi magmatic zone belong to the South belt of the Shi-Hang zone (Jiang et al., 2008; Zhu et al., 2008), including the Qitianling, the Qianlishan, the Xishan, the Jinjiling, the Huashan, and the Guposhan granite plutons (Fig. 1b). These granite plutons were emplaced in the early Yanshanian. A lithospheric extension setting is now favored for the formation of the Shi-Hang zone, especially for the South belt (Wang et al., 2003c; Li et al., 2004a; Jiang et al., 2006b, 2008; Zhu et al., 2008; Jiang et al., 2009). However, it is still unclear what tectonic processes drove the extension.

The characters of relatively high $\varepsilon_{Nd}(t)$ values and young T_{DM} model ages of these granites in the Shi-Hang zone were generally considered to be caused by involvements of a juvenile, mantle-derived magma (Gilder et al., 1996). Abundant mafic microgranular enclaves (MMEs) occur in these granites, which were also suggested as evidence for crust–mantle magma mixing (e.g. Yang et al., 2005; Zhu et al., 2006b). However, given the lack of a clear mantle signature, there are considerable discrepancies between the models proposed to explain the origin of MMEs in granite plutons (e.g. Didier and Barbarin, 1991). The reasons for relatively higher $\varepsilon_{Nd}(t)$ values of these granites in this zone still remain unclear. Identifying the specific sources that contributed to the origin of granitoids has long been a problem, because both magma mixing and wall-rock assimilation can significantly modify the whole rock chemistry. This can result in homogeneous Nd and Sr isotopic compositions in what were initially discrete components within a single pluton or batholith. Fortunately, the fine-scale zoning of zircon crystals can preserve details of the assembly of the different magmas. Recent studies have shown that trace elements and hafnium isotopic compositions of zircon can elucidate the nature of magma sources and the role of magma mixing processes in the generation of granitoids (e.g. Griffin et al., 2002; Wang et al., 2002, 2003b; Hawkesworth and Kemp, 2006; Yang et al., 2006, 2007; Zhao et al., 2010; Wong et al., 2011). Here we present the results of LA-MC-ICP-MS Hf isotopic composition of zircon from both the Cailing and Furong granites and the MMEs, together with elemental and Sr–Nd isotope data of whole rocks. These data not only allow a test of the magma-mixing hypothesis for the petrogenesis, but also fingerprint the details of origin of crust- and mantle-derived magma. This can help us to a better understanding of the geodynamic setting responsible for the formation of the Shi-Hang zone in South China.

2. Geological setting and petrography

The Qitianling granite batholith lies in southern Hunan province, South China. The southern Hunan and northern Guangxi region is located in the western part of the Nanling Mountains. The southern Hunan and northern Guangxi region demarcates the locus of the majority of Mesozoic igneous rocks and extensional basins to the southeast, contrasting with the more stable region, which is covered by the Lower Paleozoic shallow-marine carbonate and clastic sediments and the Upper Paleozoic to Middle Triassic flysch sedimentation, to the northwest. The most important deep faults here is the NE trending Chenzhou-Lingwu fault (Wang et al., 2008), which controls the distribution of the NE trending granite zone with relatively young Nd model ages and with abundant Sn–W mineralization (Fig. 1b). Based on the systematic geologic and geochemical differences of the Mesozoic basalts in both sides of the Chenzhou-Lingwu fault, Wang et al. (2008) suggested this fault as a boundary between the Yangtze Block and the Cathaysia Block during the Neoproterozoic collision.

A number of diorite and granite intrusions occur in southern Hunan and northern Guangxi region, and are distributed roughly in a NNE direction (Fig. 1b) along the Chenzhou-Lingwu fault. These diorite–granodiorite plutons, e.g. the Baoshan, the Tongshanling, the Shuikoushan, the Tongan, and the Niumiao, are of small volumes and occur as dykes, laccoliths, knobs and batholiths. They comprise predominately pyroxene diorite, biotite diorite, quartz diorite and biotite granodiorite (Wang et al., 2003c; Zhu et al., 2005). From the northeast to the southwest, the typical granitic intrusions include the Qianlishan, the Qitianling, the Jinjiling, the Xishan, the Huashan and the Guposhan granites. These granites show elliptical shapes and have a total exposed area of ca. 3000 km^2. They generally consist of porphyritic amphibole–biotite monzogranite and coarse- to medium-grained biotite granites. Basaltic rocks occur sporadically in southern Hunan province, such as the alkaline basalts of ca. 175 Ma in Ningyuan and high-Mg basalts of ca. 150 Ma in Daoxian (Zhao et al., 1998, 2001; Li et al., 2004a; Dai et al., 2008). These basaltic rocks occur as cones, pipes, sills and dykes within the Paleozoic to Lower Jurassic strata. The basalts in Ningyuan and Daoxian commonly contain a variety of lower crustal and mantle xenoliths. The major xenolith types are spinel lherzolite, dunite, pyroxenite, gabbro and garnet-bearing biotite gneisses (Dai et al., 2008).

The Qitianling pluton has an elliptical shape with a total outcrop area of 520 km^2 (Fig. 1c). Country rocks intruded by the Qitianling batholith are dominated by Permian–Carboniferous carbonate rocks and Permian–Triassic clastic sedimentary rocks. In previous studies, the Qitianling batholith was divided into three intrusive phases according to their petrographic characteristics and emplacement ages (Zheng and Jia, 2001; Zhu et al., 2009), namely, the Cailing phase, the Furong phase, and the Huangtangling phase (Fig. 1c). Many geologists have focused on studying the genesis of the complex because of its abundant economic mineralization of Sn and other metals (Bai et al., 2005; Zhao et al., 2005a,b; Jiang et al., 2006a; Li et al., 2007c).

The Cailing phase mainly occurs in the eastern, northern, and western peripheral parts of the pluton. It consists of porphyritic amphibole–biotite monzogranite. It occupies about 45% of the total exposure area of the Qitianling batholith. It has a medium-grained matrix with subhedral, normally zoned plagioclase (~30 vol.%) from An_{36} to An_{20}, K-feldspar (~30 vol.%), quartz (~30 vol.%), biotite and amphibole (Fig. 2c). Total abundance of biotite and amphibole vary from 3 vol.% to 10 vol.%. Locally amphibole can reach up to 8 vol.%. Biotite and amphibole occur as irregular relict textures replaced by quartz and palgioclase. Accessory minerals are mainly magnetite, ilmenite, zircon, apatite, monazite and titanite. K-feldspar and plagioclase megacrysts with a variable grain size (5 mm to 5 cm) are enclosed in the matrix. K-feldspar commonly shows microcline texture and Carlsbad twins. Zircon U–Pb dating indicated that the Cailing phase was emplaced at 163–160 Ma (Fu et al., 2004c; Zhu et al., 2009).

The Furong phase is also a megacrystic amphibole–biotite monzogranite and distributed in the middle and southeastern parts of the pluton. It occupies about 43% of the total exposure area of the Qitianling batholith. The rock has a medium-gained matrix composed of plagioclase, quartz, biotite and amphibole. Biotite and amphibole occur in concentrations of 5–10 vol.% and as irregular relict textures replaced by quartz and albite. The main megacrysts are K-feldspar with minor plagioclase and quartz. Magnetite, ilmenite, zircon and apatite are the main accessory minerals. The Furong phase was emplaced at 157–153 Ma (Zhao et al., 2006; Zhu et al., 2009).

The Huangtangling phase is a fine-grained granite and distributed in the middle-southern part of the pluton. It occurs as dykes and irregular bodies within the megacrystic granite. The granites of this phase occupy about 12% of the total exposure area, cutting through the Cailing and Furong granites. The rock is weakly porphyritic with phenocrysts (up to 20%) of K-feldspar and minor plagioclase. It has an allotriomorphic-granular martrix of K-feldspar, albite, quartz and biotite. Locally, tourmaline is abundant as quartz–tourmaline orbicules and veins. The phase was emplaced at 150–146 Ma (Zhu et al., 2009).

Microgranular mafic enclaves (MMEs) are widespread in the Qitianling granites, but their spatial distribution is heterogeneous, maximum concentrations occurring in some of the margins of the pluton, especially in the Cailing phase. They are most commonly subangular to subrounded (Fig. 2a–b). Enclaves are most commonly centimeters to decimeters in size, and rarely up to 2–3 m. The MMEs have mineralogical compositions ranging from quartz-diorite to tonalite. The mineralogy of MMEs is identical to that of host granites, but MMEs contain higher amounts of mafic minerals (~15 vol.% biotite and ~10 vol.% hornblende). Biotite and hornblende in MMEs commonly show resorption zones (Fig. 2d–f). Large K-feldspar and plagioclase crystals with an identical size of phenocrysts in the host also occur inside the enclaves. In some places, plagioclase crystals commonly crosscut the enclaves/host boundary (Fig. 2a–b). This suggests that the large crystals of K-feldspar and plagioclase within enclaves can be regarded as xenocrysts captured from the host magma by the enclave magma. The occurrence of xenocrysts is commonly observed in MMEs and is interpreted as proof that enclaves were in a liquid state when incorporated into a more silicic magma (e.g. Vernon et al., 1988; Perugini et al., 2003). Apatite in MMEs displays euhedral acicular habit with crystals elongated along the “c” crystallographic axis (Fig. 2f), which can be regarded as proof of a rapid cooling crystallization process. These characteristics are similar to those of MMEs originated from magma mixing (e.g. Vernon et al., 1988; Perugini et al., 2003).

3. Analytical methods

3.1. Zircon Lu–Hf isotopes

Zircons were separated from 3 samples (one from the Cailing phase and two from the MMEs in the Cailing phase) and concentrated by heavy liquid, and isodynamic magnetic separators and were then handpicked under a binocular microscope. The zircon samples were mounted in epoxy resin and polished to approximately half their thickness. Examination of internal structures was performed using cathodoluminescence (CL) imaging technique with an Electron Microprobe at Institute of Geology and Geophysics, Chinese Academy of Sciences. Internal zircon structures were investigated for information about mineral genesis and multiple growth history, which help in the interpretation of the Hf isotope data (e.g. Hoskin and Schaltegger, 2003; Wu and Zheng, 2004).

In-situ zircon Hf isotope analyses were carried out with a Geolas 193 nm Excimer laser ablation system, attached to a Multi-collector ICP-MS (Neptune) at Institute of Geology and Geophysics, Chinese

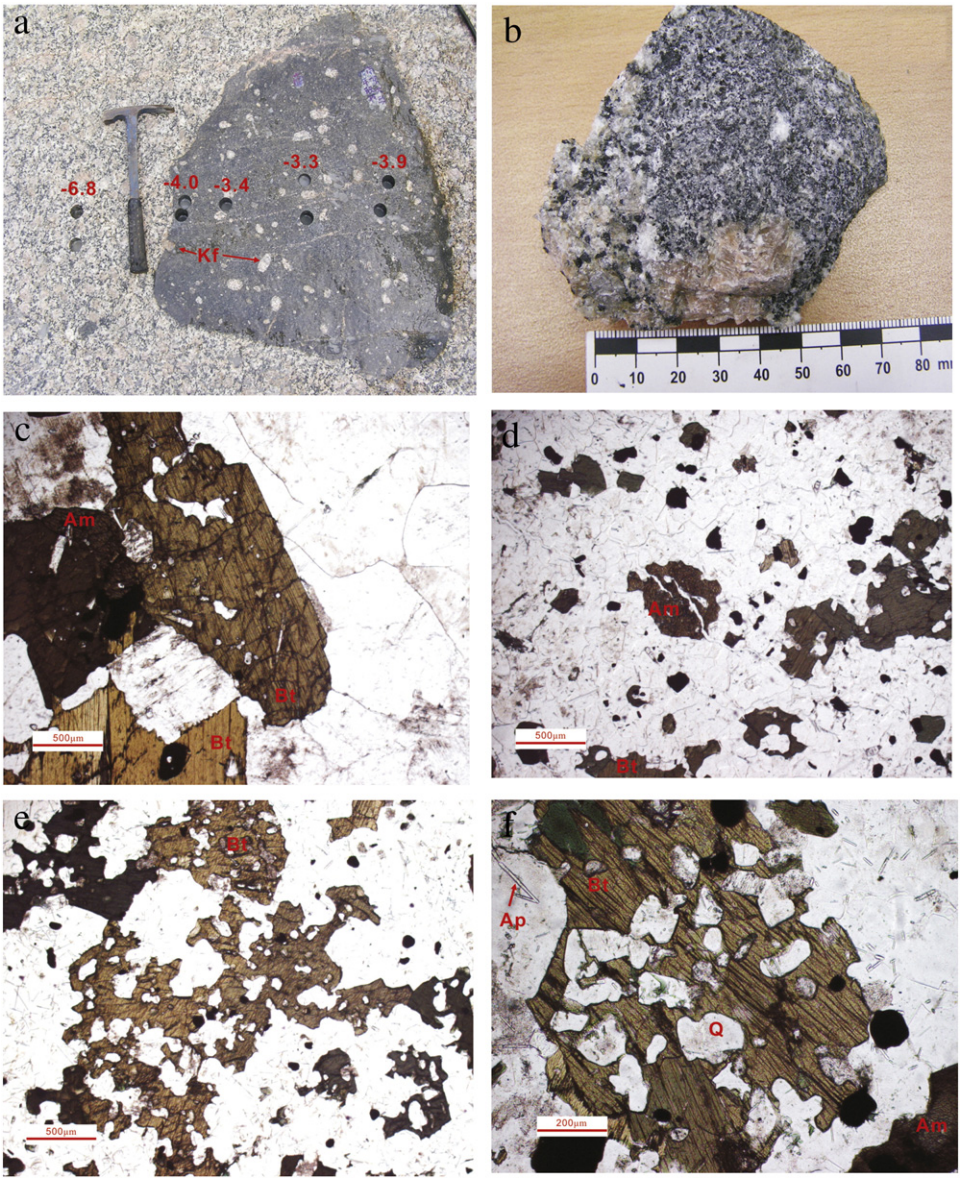

Fig. 2. (a–b) Photos of mafic enclaves in the Cailing granites. Data in (a) are the $\varepsilon_{Nd}(t)$ values of the samples from the sampling holes. (c) Microphotograph of the Cailing granites. (d–f) Microphotographs of the MMEs (Kf = K-feldspar, Am = amphibole, Bt = biotite, Q = quartz, Ap = apatite).

Academy of Sciences. Laser ablation analyses were carried out by line scan with a 32 or 63 μm laser beam sizes. A signal collection model for one block with 200 cycles, in which one cycle has 0.131 s integration time, is accepted. Isobaric interference correction was made by the methods of Xu et al. (2004) and Wu et al. (2006). The obtained $^{176}Hf/^{177}Hf$ ratio of standard zircon 91500 is 0.282316 ± 4 ($n = 45$, 2σ) in this study. The measured $^{176}Lu/^{177}Hf$ ratios of the zircons have been used here to calculate initial $^{176}Hf/^{177}Hf$ ratios. With the low Lu/Hf ratios and young ages considered here, the age corrections are very small. For the calculation of $\varepsilon_{Hf}(t)$ values, we have adopted a decay constant for ^{176}Lu of 1.865×10^{-11} year^{-1} (Scherer et al., 2001) and chondritic values of $^{176}Hf/^{177}Hf$ and $^{176}Lu/^{177}Hf$ derived by Blichert-Toft and Albarède (1997). Depleted-mantle model ages (T_{DM}) were calculated using the measured $^{176}Lu/^{177}Hf$ ratios, referred to a model depleted mantle with a present-day $^{176}Hf/^{177}Hf = 0.28325$, similar to that of average MORB (Nowell et al., 1998), and $^{176}Lu/^{177}Hf = 0.0384$ (Griffin et al., 2000). A more realistic estimation (T^{C}_{DM}) of the source rock age for the magmas was derived by projecting the initial $^{176}Hf/^{177}Hf$ of the zircon back to the depleted mantle model growth curve, assuming a mean crustal value for $^{176}Lu/^{177}Hf$ of 0.015 (GERM, 2001).

3.2. Mineral chemistry

Mineral chemistry analyses of silicates were obtained from polished thin sections using a JEOL JXA-8100 electron microprobe at State Key Laboratory for Mineral Deposits Research at Nanjing University. Operation and data processing were similar to those described by Wang et al. (2003a). Element determinations (Si, Al, Fe_{Total}, Mg, Ti, Mn, Ba, Na, K, F and Cl) of biotite, amphibole and plagioclase were carried out using a beam size of 1 μm, an accelerating potential voltage of 15 kV, and a probe current of 15 nA. Standards used were natural minerals and synthetic compounds, including hornblende (Si, Na, Mg, Al, Ca, Ti), apatite (F), barium chlorapatite (Cl), fayalite (Fe, Mn), K-feldspars (K) in the analytical procedure of silicate. Matrix effects were corrected using the ZAF software provided by JEOL. The accuracy of the reported values for the analyses is 1–5% depending on the abundance of the element.

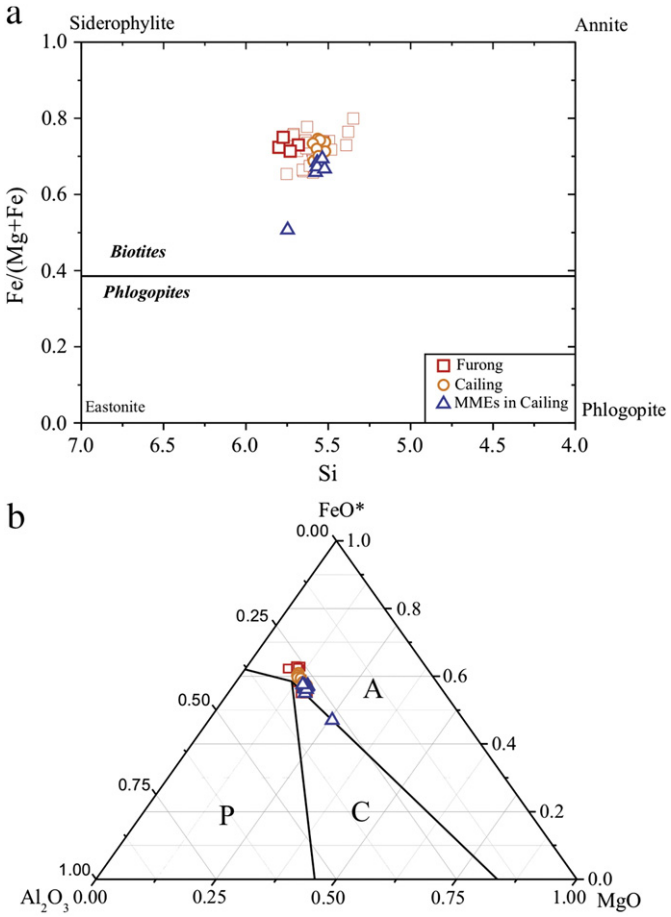

Fig. 3. (a) The classification of biotites from the Cailing and Furong granites and MMEs. (b) Plot of MgO–Al_2O_3–FeO* of biotites from the Cailing and Furong granites and MMEs (A = alkaline anorogenic suites, C = calc-alkaline orogenic suites, P = peraluminous (including S-type) suites, after Abdel-Rahman, 1994).
Data of the Furong granite are from Zhao et al. (2005b).

3.3. Major and trace element contents of whole rocks

Major element compositions of whole rocks were analyzed using an ICP-AES at State Key Laboratory for Mineral Deposits Research at Nanjing University after alkaline fuse digestion, with analytical uncertainties better than 0.5% for all major elements. Trace element contents were determined by a Finnigan MAT Element II HR-ICP-MS at the same laboratory, and the analytical procedures are similar to those described by Gao et al. (2003). About 50 mg of powdered sample was dissolved in high-pressure Teflon bombs using a HF + HNO_3 mixture. Rh was used as an internal standard to monitor signal drift during ICP-MS measurement. The USGS rock standards GSP-1 and AGV-2 were chosen for calibrating element concentrations of the measured samples. Analytical uncertainties were lower than 10%.

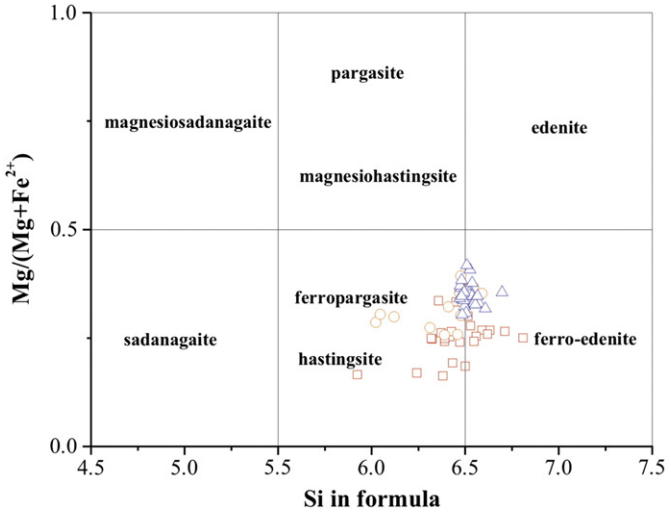

Fig. 4. The classification of amphiboles from the Cailing and Furong granites and MMEs (after Hawthorne and Oberti, 2007). Data of the Furong granite are from Zhao et al. (2005b). Symbols are as in Fig. 3.

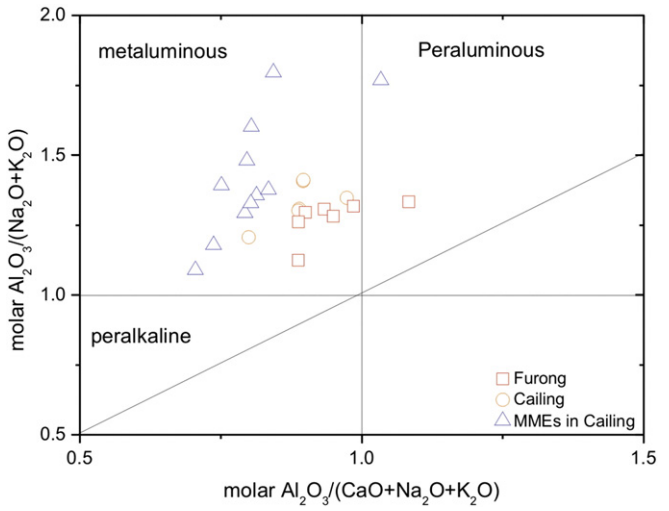

Fig. 5. A/NK vs. A/CNK plot showing the metaluminous nature of the Cailing and Furong granites and MMEs.

3.4. Sr–Nd isotopic compositions of whole rocks

Sr and Nd isotope analyses of the whole rock samples were done using the following chemical separation and mass spectrometry methods. About 100 mg sample was dissolved in the same way for trace element analyses. Complete separation of Sr was achieved by a combination of cation-exchange chromatography in H^+ form and pyridinium form with the DCTA complex. Nd was then separated from the REE fractions by cation-exchange resin using HIBA as eluent. The detailed separation procedures and mass spectrometry analyses were the same as those described by Pu et al. (2004, 2005). The separated

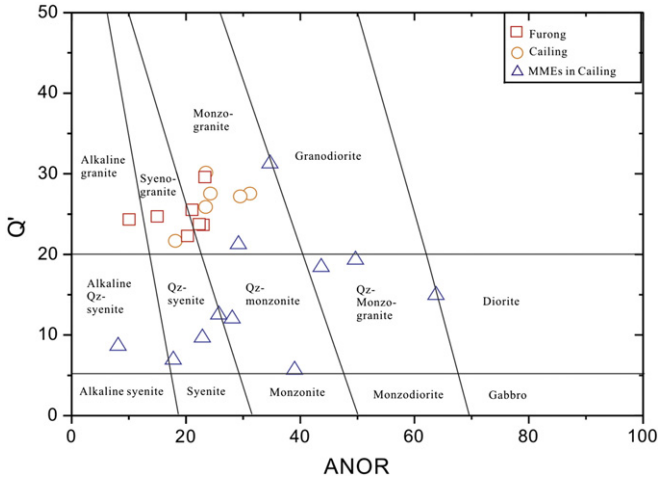

Fig. 6. Q′-ANOR normative composition diagram (after Streckeisen and Le Maitre, 1979) for classification of the Cailing and Furong granites and MMEs. Q′ = Q/(Q + Or + Ab + An) × 100; ANOR = An/(Or + An) × 100.

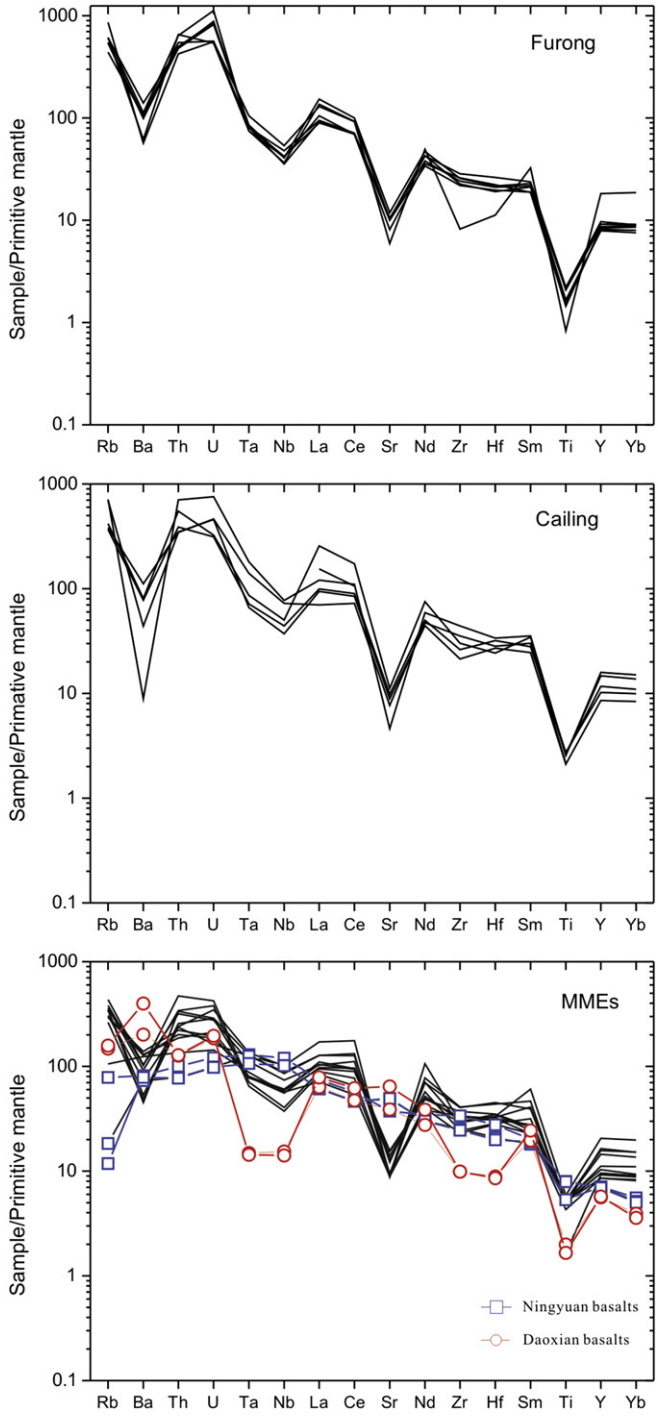

Fig. 7. Primitive mantle-normalized trace element spidergram for the Cailing and Furong granites and MMEs. The normalization values are from Sun and McDonough (1989). The data of the Ningyuan basalts and the Daoxian basalts are from Li et al. (2004a).

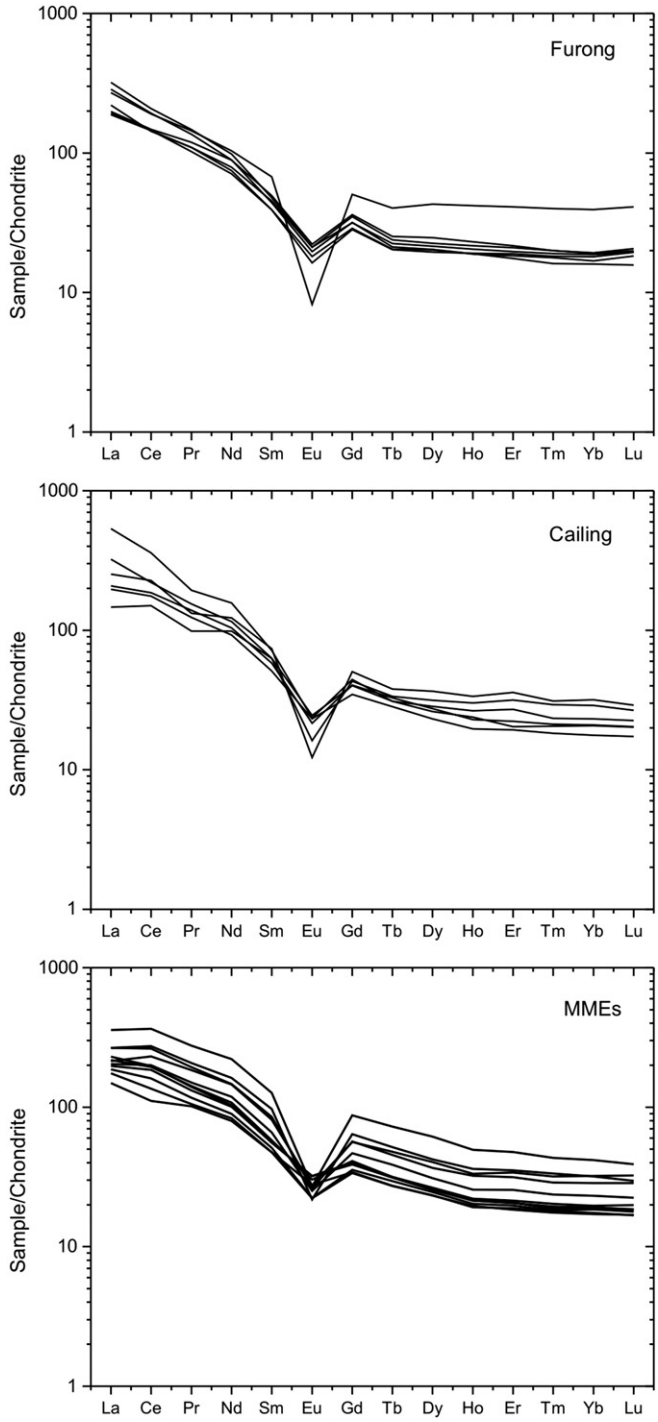

Fig. 8. Chondrite-normalized REE diagrams for the Cailing and Furong granites and MMEs. The normalization values are from Boynton (1984).

Sr sample was dissolved in 1 μl of 1 N HCl and then loaded with TaF_5 solution onto W filament. The separated Nd sample was dissolved in 1 μl of 1 N HCl and then loaded with H_3PO_4 solution onto Re double-filament. Determination of Sr and Nd isotopic composition was carried out by a Finnigan MAT Triton TI TIMS in Nanjing University. The Sr isotopic data are normalized to $^{86}Sr/^{88}Sr = 0.1194$. The Nd isotopic data are normalized to $^{146}Nd/^{144}Nd = 0.7219$. The NIST 987 Sr solution standard gave an average value of 0.710260 ± 0.000006 ($n = 10$, 2σ) in this study. The JNDi-1 Nd standard gave an average value of 0.512120 ± 0.000005 ($n = 15$, 2σ), which is similar to the referenced value of 0.512115 ± 0.000007 (Tanaka et al., 2000).

4. Results

4.1. Mineral chemistry

Representative electron microprobe analyses and chemical formulae calculated for biotite from the Cailing granites and MMEs are listed in e-component Appendix Table 1. The biotites display high FeO contents (>25%), TiO_2 contents (>1%) and high Fe/(Fe + Mg) ratios (>0.5). According to the mica classification, all of them are close to the Fe-rich siderophyllite–annite end-member (Fig. 3a). As shown in the plot of MgO–Al_2O_3–FeO (Fig. 3b), all data of the biotite fall in A-

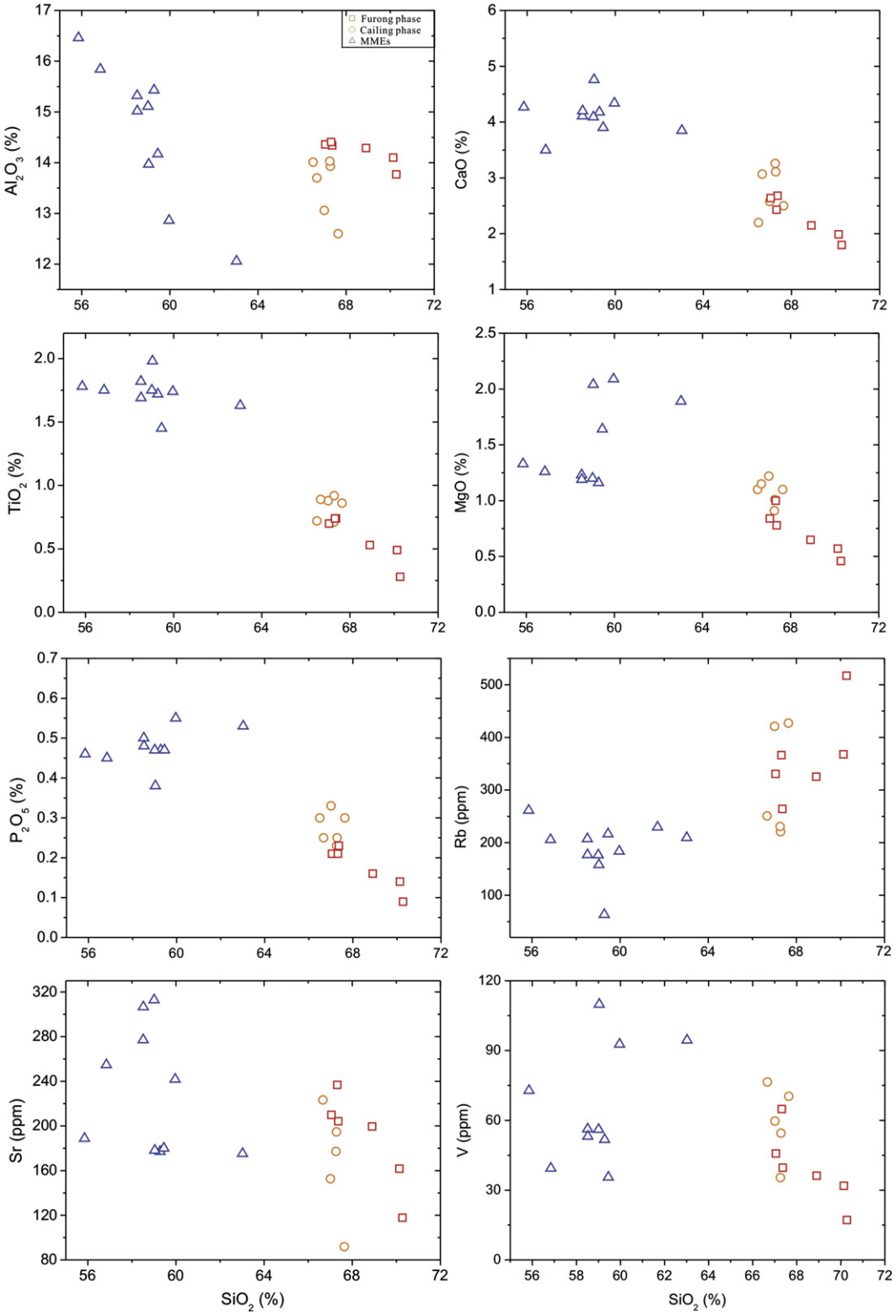

Fig. 9. Selected major oxide (wt.%) and trace elements (ppm) vs. SiO_2 (wt.%) for the Cailing and Furong granites and MMEs.

type region (anorogenic alkaline granite) of Abdel-Rahman (1994). The chemical compositions of biotite in the Cailing phase are similar to those in the Furong phase (Zhao et al., 2005b). Biotites in the MMEs have significantly higher MgO contents (6.86–11.58%) and lower TiO_2 (0.95–4.09%) than those in host granites (MgO: 5.48–7.22%, TiO_2: 2.59–4.45%).

Selected amphibole compositions and chemical formulae calculated are listed in e-component Appendix Table 2. The studied amphiboles in the Cailing granites and in MMEs belong to calcic amphibole. According to the nomenclature of Hawthorne and Oberti (2007) for calcic amphibole, they are ferropargasite and ferro-edenite hornblende (Fig. 4). All amphibole compositions plot in the field of 'magmatic'

amphibole, i.e. above the line $(Ca + {}^{IV}Al) = 2.5$ as proposed by Giret et al. (1980). Amphiboles in MMEs generally have higher MgO contents (5.55–7.37%) than those in host granites (4.47–6.97%).

Plagioclase in host granites is mainly oligoclase and andesine with Ab contents of 68.3–81.1%, An contents of 17.2–28.2% and Or contents of 1.7–3.5% (e-component Appendix Table 3). Plagioclase in MMEs shows distinctly oscillatory zoning. The An contents in plagioclase cores generally are higher (30.5–34.6%) than those in rims (13.1–27.6%).

4.2. Major and trace elements

The Cailing phase granites have a narrow variation of chemical compositions (e-component Appendix Table 4), with SiO_2 contents from 66.50% to 67.28%, Al_2O_3 contents from 12.60% to 14.03%, TiO_2 contents from 0.71% to 0.92%, respectively. Total $K_2O + Na_2O$ contents vary from 7.38% to 8.77%. The granites are metaluminous with A/CNK (molar ratio of $Al_2O_3/[CaO + Na_2O + K_2O]$) ranging from 0.80 to 0.97 (Fig. 5). The Furong phase granites have SiO_2 contents ranging from 67.05 to 70.28%. They have higher Al_2O_3 (13.77–15.12%) and lower TiO_2 (0.28–0.74%) than the Cailing phase. Total $K_2O + Na_2O$ contents vary from 8.21% to 9.57%. They are mostly metaluminous with A/CNK ranging from 0.89 to 0.98, although one sample (GT-4-4) is slightly peraluminous (Fig. 5). All granite samples from the Cailing phase and the Furong phase range from alkaline granite to monzogranite in Q′-ANOR plot (Fig. 6). These granites are characterized by high contents of large ion lithospheric elements (LILE) such as Rb, Th, U, Pb and high field strength elements (HFSE) such as Nb, Ta, Zr, Hf, and high REE and Y (Fig. 7). Chondrite-normalized REE patterns of the granites show relative enrichment of light rare earth elements (LREEs), with high $(La/Yb)_N$ ratios (5.07–23.13) and significant negative Eu anomalies (Fig. 8).

The MMEs have SiO_2 contents ranging from 55.85% to 63.02% with higher TiO_2 (1.45–1.98%, except one with 0.55%), CaO contents (3.50–6.08%) and MgO contents (1.16–2.09%) than those of the host granites (e-component Appendix Table 4). They also have higher contents of Fe_2O_3, MnO, P_2O_5, Zr, Hf, Nb and Ta, but lower contents of Rb, U and Th (Fig. 7). Total $K_2O + Na_2O$ contents vary from 6.12% to 9.99%. The MMEs range from alkaline syenite to quartz monzogranite (Fig. 6). Chondrite-normalized REE patterns of the MMEs are marked by enrichment in the LREEs and negative Eu anomalies, similar to those of host granites (Fig. 8). In the primitive mantle-normalized trace element variation diagram (Fig. 7), the MMEs are characterized by high contents of large ion lithospheric elements (LILE) such as Rb, Th, U, high field strength elements (HFSE) such as Nb, Ta, Zr, Hf, and negative anomalies in Ba, Sr and Ti, similar to the host granites. On binary major and trace element vs. SiO_2 variation diagrams (Fig. 9), samples from the MMEs and granites are discontinuous and do not show linear trends as might be expected if the enclaves represented restites.

Zircon saturation temperatures (T_{Zr}) calculated from bulk-rock compositions provide minimum estimates of magma temperature (Watson and Harrison, 1983). Calculated T_{Zr} of the Cailing and Furong granites are mostly in the range of 772–858 °C. Calculated T_{Zr} of the MMEs vary from 740 to 824 °C.

4.3. Sr–Nd isotopes

The initial $^{87}Sr/^{86}Sr$ ratios and $\varepsilon_{Nd}(t)$ values have been calculated at 160 Ma on the basis of zircon U–Pb dating of the rocks and the data are listed in Table 1. The Cailing granites have variable $^{87}Rb/^{86}Sr$ (3.28–14.48) and $^{87}Sr/^{86}Sr$ (0.7176–0.7409) ratios. The samples have age-corrected $(^{87}Sr/^{86}Sr)_i$ ratios ranging from 0.7091 to 0.7110. We noted that these $(^{87}Sr/^{86}Sr)_i$ ratios bear large uncertainties due to very high Rb/Sr ratios and they do not form an isochron. The granites have fairly constant Nd isotopic compositions and $\varepsilon_{Nd}(t)$ values vary from −6.8 to −5.8. Two-stage model ages vary from 1.39 Ga to 1.50 Ga. Age-corrected $(^{87}Sr/^{86}Sr)_i$ ratios of the Furong granites vary from 0.7108 to 0.7132. $\varepsilon_{Nd}(t)$ values of the samples vary from −7.6 to −6.6 and calculated T_{DM} ages range from 1.48 Ga to 1.56 Ga.

The MMEs have variable $^{87}Rb/^{86}Sr$ (1.03–4.01) and $^{87}Sr/^{86}Sr$ (0.7126–0.7195) ratios, and $(^{87}Sr/^{86}Sr)_i$ ratios vary from 0.7091 to 0.7121. The samples have variable $\varepsilon_{Nd}(t)$ values (−6.7 to −3.3). Calculated T_{DM} ages vary from 1.21 Ga to 1.49 Ga. Generally, $\varepsilon_{Nd}(t)$ values of the MMEs with small size are similar to those of host rocks. However, samples from a mafic enclave with a diameter of about 0.5 m have higher $\varepsilon_{Nd}(t)$ values than host granites. From the rim to the central part in this enclave, $\varepsilon_{Nd}(t)$ values gradually increase (Fig. 2).

4.4. Zircon Hf isotopes

Twenty-one spots from sample QTL-13 (from the Cailing granite) are analyzed for Lu–Hf isotopic compositions (Table 2). Most spots

Table 1
Sr–Nd isotope compositions of the Cailing and Furong granites and MMEs.

	Sample	Rb (ppm)	Sr (ppm)	$^{87}Rb/^{86}Sr$	$^{87}Sr/^{86}Sr$	Error	$(^{87}Sr/^{86}Sr)_i$	Sm (ppm)	Nd (ppm)	$^{147}Sm/^{144}Nd$	$^{143}Nd/^{144}Nd$	Error	$\varepsilon_{Nd}(t)$	T^2_{DM} (Ma)
Furong	FR-63	264.1	204.2	3.75	0.719366	0.000003	0.711327	9.63	53.4	0.1092	0.512196	0.000004	−6.9	1506
	FR-33	330.7	209.9	4.56	0.720631	0.000004	0.710837	8.82	47.4	0.1125	0.512217	0.000002	−6.6	1478
	FR-43							7.65	42.6	0.1087	0.512176	0.000003	−7.3	1537
	GT-4-4	367.1	204.2	5.21	0.724336	0.000004	0.713153	8.59	53.5	0.0971	0.512151	0.000004	−7.6	1558
Cailing	QTL-6	220.9	194.8	3.28	0.717996	0.000004	0.710946	11.33	62.4	0.1098	0.512202	0.000009	−6.8	1497
	QTL-14	230.6	177.2	3.77	0.719080	0.000003	0.710990	9.98	55.5	0.1088	0.512233	0.000003	−6.2	1447
	QT-27	427.2	91.8	14.48	0.740856	0.000026	0.709783							
	QT-29	421.0	152.7	3.93	0.717556	0.000024	0.709130	12.22	59.1	0.1285	0.512288	0.000020	−5.5	1391
	QT-38							13.98	94.0	0.0612	0.512209	0.000020	−5.8	1410
MMEs	QTL-1-B	209.2	175.1	3.46	0.719528	0.000003	0.712100	18.93	97.2	0.1178	0.512218	0.000005	−6.7	1485
	QTL-2	183.8	241.7	2.20	0.716026	0.000034	0.711301	16.61	88.1	0.1141	0.512235	0.000004	−6.3	1452
	QTL-3	216.6	180.0	3.48	0.718466	0.000003	0.710988	9.26	49.9	0.1123	0.512237	0.000003	−6.2	1446
	QTL-5	205.6	254.6	2.34	0.716450	0.000002	0.711432	12.84	71.3	0.1090	0.512285	0.000002	−5.2	1365
	QTL-7	207.1	277.1	2.16	0.714963	0.000019	0.710318	11.28	64.8	0.1053	0.512341	0.000003	−4.0	1270
	QTL-8	63.2	177.1	1.03	0.712821	0.000003	0.710604	9.26	47.8	0.1173	0.512383	0.000014	−3.4	1222
	QTL-9	176.6	312.8	1.63	0.712570	0.000004	0.709062	10.84	61.9	0.1060	0.512378	0.000003	−3.3	1213
	QTL-10							10.88	60.4	0.1090	0.512354	0.000002	−3.9	1255
	QTL-11	229.5	180.1	3.69	0.718748	0.000002	0.710828	9.97	53.6	0.1125	0.512259	0.000025	−5.8	1411
	QTL-12	261.2	188.7	4.01	0.718973	0.000003	0.710370	15.88	87.0	0.1104	0.512240	0.000004	−6.1	1438
	QTL-15	157.9	178.0	2.57	0.716229	0.000005	0.710716	24.66	132.9	0.1122	0.512250	0.000002	−5.9	1425

—Data of QT-27, QT-29, QT-38 are from Zhu et al. (2003).

Table 2
Lu–Hf isotope compositions of zircons from the Cailing granite (QTL-13) and MMEs (QTL-2 and QTL-4).

Spot	$^{176}Lu/^{177}Hf$	$^{176}Hf/^{177}Hf$	Error	Age (Ma)	$(^{176}Hf/^{177}Hf)_i$	$\varepsilon_{Hf}(t)$	T_{DM} (Ga)	T^C_{DM} (Ga)
QTL-13								
1	0.000632	0.282521	0.000024	160	0.282519	−5.4	1.03	1.55
2	0.000750	0.282508	0.000026	160	0.282506	−5.9	1.05	1.58
3	0.000518	0.282537	0.000017	160	0.282535	−4.9	1.00	1.51
4	0.000656	0.282504	0.000021	160	0.282502	−6.0	1.05	1.59
5	0.000619	0.282519	0.000021	160	0.282517	−5.5	1.03	1.55
6	0.000663	0.282514	0.000022	160	0.282512	−5.7	1.04	1.57
7	0.000609	0.282541	0.000018	160	0.282539	−4.7	1.00	1.50
8	0.001187	0.282509	0.000021	160	0.282505	−5.9	1.06	1.58
9	0.000737	0.282452	0.000022	160	0.282450	−7.9	1.12	1.70
10	0.000679	0.282546	0.000020	160	0.282544	−4.6	0.99	1.49
11	0.000772	0.282553	0.000022	160	0.282551	−4.3	0.98	1.48
12	0.000627	0.282542	0.000025	160	0.282540	−4.7	1.00	1.50
13	0.000862	0.282557	0.000023	160	0.282554	−4.2	0.98	1.47
14	0.001339	0.282569	0.000028	160	0.282565	−3.8	0.98	1.45
15	0.000611	0.282512	0.000020	160	0.282510	−5.8	1.04	1.57
16	0.000504	0.282514	0.000018	160	0.282512	−5.7	1.03	1.56
17	0.000826	0.282576	0.000022	160	0.282574	−3.5	0.95	1.43
18	0.000836	0.282570	0.000021	160	0.282568	−3.7	0.96	1.44
19	0.000519	0.282517	0.000018	160	0.282515	−5.6	1.03	1.56
20	0.000471	0.282531	0.000021	160	0.282530	−5.1	1.01	1.53
21	0.000505	0.282451	0.000020	160	0.282449	−7.9	1.12	1.70
QTL-2								
1	0.001184	0.282616	0.000026	160	0.282612	−2.1	0.91	1.34
2	0.000688	0.282525	0.000023	160	0.282523	−5.3	1.02	1.54
3	0.000650	0.282417	0.000024	160	0.282415	−9.1	1.17	1.78
4	0.000867	0.282590	0.00002	160	0.282587	−3.0	0.93	1.40
5	0.001398	0.282713	0.000025	160	0.282709	1.3	0.77	1.13
6	0.000712	0.282536	0.000021	160	0.282534	−4.9	1.01	1.52
7	0.000663	0.282509	0.000022	160	0.282507	−5.9	1.04	1.58
8	0.000966	0.282618	0.000037	160	0.282615	−2.0	0.90	1.34
9	0.000702	0.282595	0.000023	160	0.282593	−2.8	0.92	1.38
10	0.001267	0.282687	0.000055	160	0.282683	0.4	0.81	1.18
11	0.001173	0.282612	0.000031	160	0.282608	−2.3	0.91	1.35
12	0.001441	0.282722	0.000064	160	0.282718	1.6	0.76	1.11
13	0.000902	0.282755	0.000084	160	0.282752	2.8	0.70	1.03
14	0.001290	0.282560	0.000018	160	0.282556	−4.1	0.99	1.47
15	0.001172	0.282599	0.000022	160	0.282595	−2.7	0.93	1.38
16	0.000512	0.282534	0.000017	160	0.282532	−5.0	1.00	1.52
17	0.000967	0.282555	0.000026	160	0.282552	−4.3	0.99	1.48
18	0.001471	0.282463	0.000025	160	0.282459	−7.6	1.13	1.68
19	0.001318	0.282642	0.000038	160	0.282638	−1.2	0.87	1.28
20	0.001635	0.282553	0.000025	160	0.282548	−4.4	1.01	1.48
21	0.000917	0.282561	0.000023	160	0.282558	−4.1	0.98	1.46
QTL-4								
1	0.002164	0.282595	0.000034	160	0.282589	−3.0	0.96	1.39
2	0.000577	0.282541	0.000032	160	0.282539	−4.7	1.00	1.50
3	0.000569	0.282499	0.000021	160	0.282497	−6.2	1.05	1.60
4	0.001033	0.282543	0.000019	160	0.282540	−4.7	1.01	1.50
5	0.000618	0.282543	0.000025	160	0.282541	−4.7	0.99	1.50
6	0.001286	0.282650	0.000044	160	0.282646	−0.9	0.86	1.27
7	0.000733	0.282520	0.000022	160	0.282518	−5.5	1.03	1.55
8	0.000511	0.282507	0.000022	160	0.282505	−5.9	1.04	1.58
9	0.000880	0.282575	0.000026	160	0.282572	−3.6	0.96	1.43
10	0.000768	0.282540	0.000027	160	0.282538	−4.8	1.00	1.51
11	0.001711	0.282618	0.000030	160	0.282613	−2.1	0.92	1.34
12	0.001038	0.282618	0.000030	160	0.282615	−2.0	0.90	1.34
13	0.000602	0.282659	0.000023	160	0.282657	−0.6	0.83	1.24
14	0.000890	0.282708	0.000029	160	0.282705	1.2	0.77	1.13
15	0.000660	0.282511	0.000030	160	0.282509	−5.8	1.04	1.57
16	0.000697	0.282702	0.000028	160	0.282700	1.0	0.77	1.15
17	0.000492	0.282127	0.000028	160	0.282126	−19.4	1.57	2.42
18	0.000695	0.282746	0.000028	160	0.282744	2.5	0.71	1.05
19	0.000605	0.282715	0.000030	160	0.282713	1.4	0.75	1.12
20	0.000747	0.282591	0.000025	160	0.282589	−3.0	0.93	1.39
21	0.000864	0.282697	0.000022	160	0.282694	0.8	0.78	1.16

are the same locations as those for SHRIMP analyses. The others lie on the rims and show occasional zones in CL images. The $^{176}Hf/^{177}Hf$ ratios vary from 0.282451 to 0.282576. The calculated $(^{176}Hf/^{177}Hf)_i$ vary from 0.282450 to 0.282574 and $\varepsilon_{Hf}(t)$ vary from −8.1 to −3.7, with a maximum peak at −5.5 (Fig. 10). Calculated two-stage T^C_{DM} ages vary from 1.43 Ga to 1.71 Ga.

Twenty-one spots from sample QTL-2 (from the MMEs) are analyzed (Table 2). They have variable ratios of $(^{176}Hf/^{177}Hf)_i$, from 0.282415 to

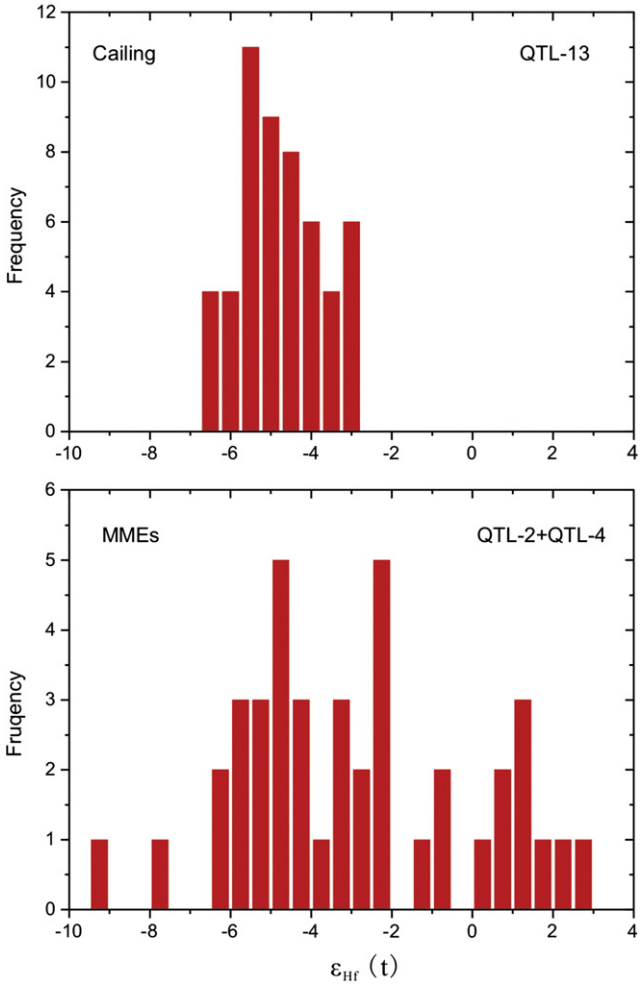

Fig. 10. Histogram of zircon $\varepsilon_{Hf}(t)$ values of the Cailing granites and MMEs.

0.282752. $\varepsilon_{Hf}(t)$ values vary from −9.2 to +2.6 and T_{DM}^{C} ages range from 1.03 Ga to 1.78 Ga. Twenty spots from sample QTL-4 also give variable ratios of $(^{176}Hf/^{177}Hf)_i$ from 0.282497 to 0.282744. $\varepsilon_{Hf}(t)$ values vary from −6.4 to +2.3 and T_{DM}^{C} ages vary from 1.05 Ga to 1.60 Ga. In histogram plots (Fig. 10b), $\varepsilon_{Hf}(t)$ values of the MMEs can be separated into two groups. One group concentrates at −5.0 and the other group concentrates at +1.5. Such Hf isotopic characteristics are likely indicative of a binary mixing between a juvenile, mantle-derived magma, and an older crustal component (Griffin et al., 2002; Li et al., 2007b).

5. Discussion

5.1. Petrogenetic type: S-type, I-type or A-type?

Since the introduction of the terms I-type and S-type granite by Chappell and White (1974), granitic rocks have commonly been divided into I-, S-, M- and A-types according to the nature of their protolith and their geneses. Later on, Eby (1992) proposed that the A-type could be further divided into A_1 and A_2 subtypes. However, the distinction between different types is not always straightforward. Several attempts have been made to discriminate A-type from the others (Collins et al., 1982; Whalen et al., 1987; Eby, 1990, 1992). Generally, the S-type granites are calc-alkaline with ASI > 1.1, whereas the A-type granites belong to alkaline and peralkaline series. Petrographically, the S-type granites contain abundant Al-rich minerals such as muscovite, garnet and cordierite (Zen, 1988; Clemens, 2003; Ishihara, 2007), whereas the mafic minerals in A-type granites generally include Fe-rich biotite and calcic amphibole for the A_2 type subtype or sodic amphibole and pyroxene for the A_1 subtype (Bonin, 2007). Therefore, the Qitianling granites should not be classified as S-type (e.g. Wang et al., 2003c). It is not easy to distinguish the A-type and the highly fractionated I-type granites (King et al., 2001; Wu et al., 2003; Li et al., 2007a). However, in terms of trace element composition, the A-type granites are comparatively enriched in alkaline and HFSE elements, such as Zr, Nb, Y, REE and Ga.

The Cailing and Furong phases from the Qitianling batholith have most characteristics of A-type granites. They contain Fe-rich biotite and calcic amphibole. They have high $K_2O + Na_2O$ (7.38–9.57%) and FeO*/MgO ratios (3–7) (Fig. 11). They also have high REE contents, HFSE contents and high 10^4 Ga/Al ratios (2.79–3.28). In the discrimination diagrams of $K_2O + Na_2O$ vs. 10^4 Ga/Al and total FeO*/MgO vs. Zr + Nb + Ce + Y, all of them fall in the field of A-type granites (Fig. 12). These geochemical characteristics strongly suggest an A-type affinity for the Cailing and Furong granites. High Rb/Nb and Y/Nb ratios of these rocks further suggest that they belong to the A_2 group of Eby (1992) (Fig. 12).

The other granites outcropped in southern Hunan and northern Guangxi area in the Shi-Hang zone (Fig. 1b), such as the Huashan, Guposhan, Xishan, Jinjiling and Qianlishan granites, share the similar mineral assemblages, mineral compositions and geochemical characteristics

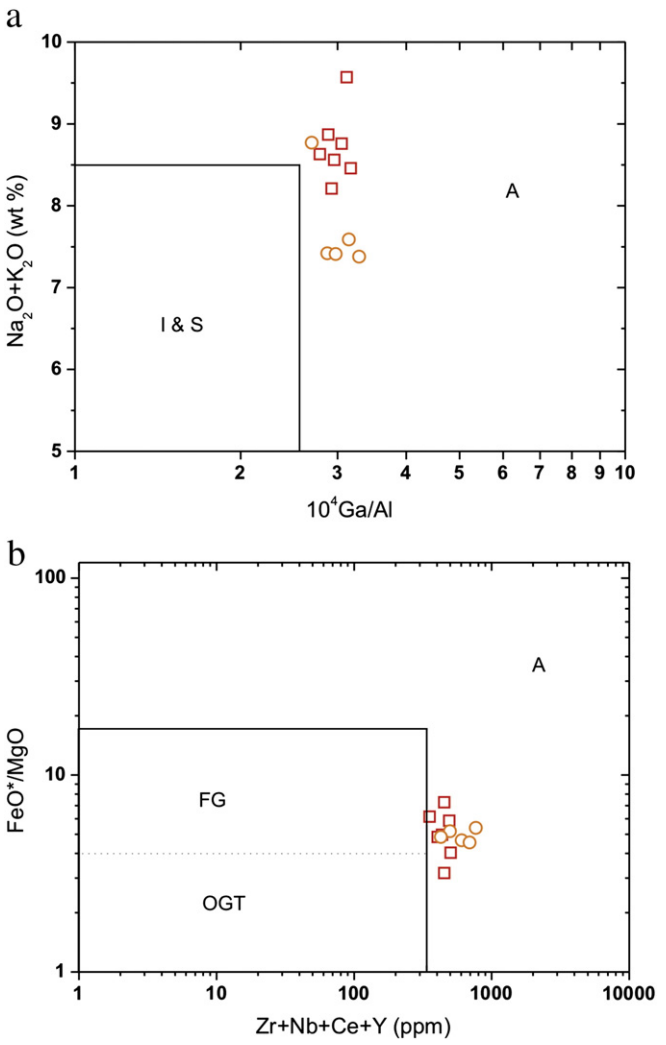

Fig. 11. (a) $K_2O + Na_2O$ vs. 10^4 Ga/Al and (b) FeO*/MgO vs. Zr + Nb + Ce + Y classification diagram of Whalen et al. (1987) for the Cailing and Furong granites. FG = fractionated M-, S- and I-type felsic granites; OGT = unfractionated M-, S- and I-type granites. Symbols are as in Fig. 3.

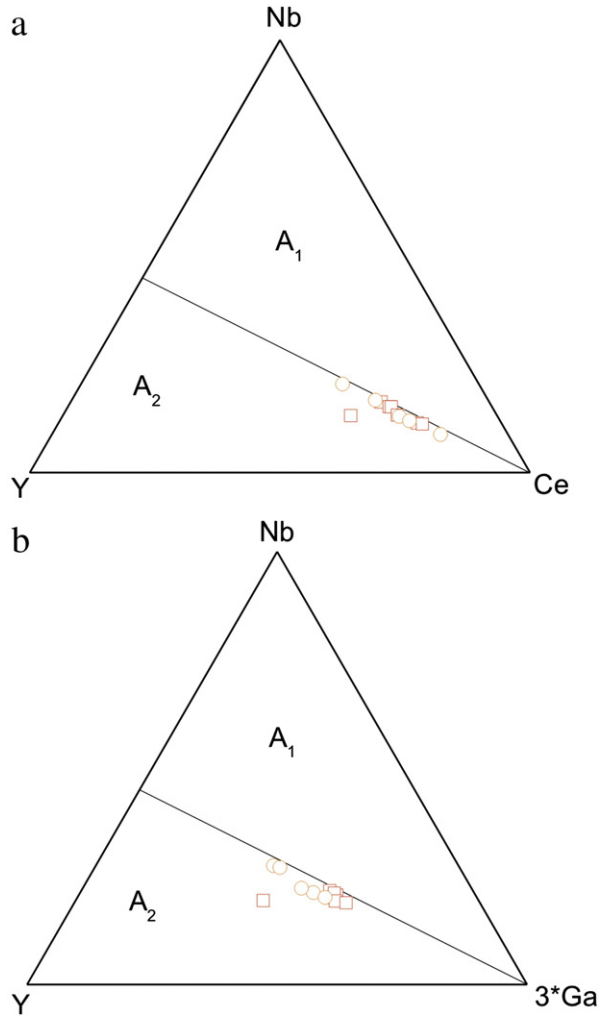

Fig. 12. Plots of the Cailing and Furong granites in (a) Nb–Y–Ce and (b) Nb–Y-3*Ga diagram of Eby (1992) for subdivision of A_1-type and A_2-type granites. Symbols are as in Fig. 3.

with the Qitianling granites (Fu et al., 2005; Zhu et al., 2006a; Jiang et al., 2006b; also see reviews by Jiang et al., 2008 and Zhu et al., 2008). All these granites have A-type characteristics and form a NNE-trending A-type granite belt (Fig. 1b).

5.2. Origin of MMEs

Mafic Microgranular enclaves (MMEs) are widespread in granitic rocks and have been the focus of many studies on magma mixing (see reviews by Didier and Barbarin, 1991). However, there are considerable discrepancies between the models proposed to explain the origin of MMEs, including whether they are restites of source rocks (Chappell et al., 1987; White et al., 1999), wall-rock xenoliths (Maas et al., 1997), early crystal-melt segregations (Dahlquist, 2002; Donaire et al., 2005) or products of mixing and mingling of different sources-derived magmas (Vernon, 1984; Didier and Barbarin, 1991; Perugini et al., 2003; Barbarin, 2005; Guan et al., 2011).

The enclaves in the Qitianling granites have igneous microtextures and contain acicular apatites, which are analogous to other cases from around the world (Vernon, 1984; Didier and Barbarin, 1991). Acicular apatite habits are common in comingled mafic pillows (Vernon et al., 1988) and have been attributed to rapid cooling, the result of mingling of small volumes of hot basalt with a cool granitic melt (Sparks and Marshall, 1986). Also, the presence of megacrysts, such as K-feldspar, in the enclaves implies that the enclaves are hybrids. These observations constitute direct evidence to argue against the interpretation that these mafic enclaves are restites or xenoliths. Instead, both the granites and the mafic enclaves originated from magmas that were commingled to various degrees.

Although mafic enclaves have different major element contents than the host granites, they exhibit very similar trace element, mineral chemical compositions with respect to their host. This point was often used to argue against magma mixing hypothesis. These mafic enclaves might be formed by crystal–liquid differentiation mechanisms operating within a single, parental granitic magma (Dahlquist, 2002; Donaire et al., 2005). Isotopes can be used to distinguish these processes. Some samples from mafic enclaves with small sizes have similar Sr–Nd isotopic compositions as their host granites. However, samples from mafic enclaves with large sizes display different $\varepsilon_{Nd}(t)$ values from their host granites. From the center to the rim of the enclaves, $\varepsilon_{Nd}(t)$ values gradually decrease (Fig. 2a). We conclude that the similarity of trace elemental and isotopic compositions between mafic enclaves and host granites was caused by diffusion and partial re-equilibration.

Zircons can better record the primary information of magma due to earlier crystallization and higher closure temperature of Lu–Hf isotopic system. Zircons from the Cailing granite have the same crystallization ages as those from the MMEs. But they display different $\varepsilon_{Hf}(t)$ values (Fig. 10). $\varepsilon_{Hf}(t)$ values of zircons from the Cailing granite vary from −8.1 to −3.7, with a maximum at −5.5. Zircons from the MMEs have $\varepsilon_{Hf}(t)$ values ranging from −6.4 to +2.3. $\varepsilon_{Hf}(t)$ values can be separated into two groups. One group has a maximum peak at −5.0, similar to the granites, whereas the other group abundance maximum peak at about +1.5. The difference in $\varepsilon_{Hf}(t)$ values between the MMEs and host granites indicates that they formed from different sources. Therefore, the MMEs in the Qitianling granites cannot have originated from early crystal segregation. Thus, Hf isotopes provide the most direct evidence for mixing processes between mafic and felsic magmas, which were likely derived from different sources.

The mafic magma has been contaminated by felsic magma during the mixing process, as can be demonstrated by petrography and Sr–Nd isotopic compositions. K-feldspar phenocrysts within the MMEs can be regarded as xenocrysts captured from the host felsic magma. Mafic minerals within MMEs often show resorption textures. Elemental and Sr–Nd isotopic compositions of MMEs tend to be consistent with their host granites. Thus, it is difficult to directly constrain the sources of mafic magma. There are many Jurassic basaltic and alkaline igneous rocks occurring in the studied area, i.e. the Ningyuan alkaline basalt of ca. 175 Ma in age, syenitic intrusions of ca. 160 Ma and the Daoxian high-Mg basalt of ca. 150 Ma. They originated from partial melting of the asthenospheric or the lithospheric mantle. The Ningyuan alkaline basalt have OIB-type trace elemental characteristics and depleted isotopic compositions ($\varepsilon_{Nd}(t) = \sim +5$). They were suggested to have formed by small degrees of melting of the asthenosphere (Li et al., 2004a). The Daoxian high-Mg tholeiite basalt is depleted in Nb and Ta, similar to arc basalt. The basalt has enriched isotopic compositions ($\varepsilon_{Nd}(t) = \sim -2$), and has been suggested to have formed from melting of an enriched lithospheric mantle source (Li et al., 2004a). The MMEs in the Qitianling granite are enriched in LILE (K, Rb), REE, HFSE (Th, U, Hf, Zr, Nb, Ta), which are similar to the Ningyuan alkaline basalt and are different from the Daoxian basalts (Fig. 7). We thus infer that the mafic magma of the MMEs originated from the same source as the alkaline basalt. This is further supported by studies on MMEs in the Guposhan granites which have zircon $\varepsilon_{Hf}(t)$ values of ~+7.4 (Zhao et al., 2010).

5.3. Petrogenetic model of the Cailing and Furong granites

Several petrogenetic models for A-type magmas have been proposed: (1) direct fractionation products of mantle-derived alkaline basalts (e.g., Turner et al., 1992; Litvinovsky et al., 2002; Mushkin et

al., 2003); (2) partial melting of specific crustal protoliths (e.g. Collins et al., 1982; Whalen et al., 1987; Creaser et al., 1991); (3) hybridization between anatectic granitic and mantle-derived mafic magmas (Kerr and Fryer, 1993; Wickham et al., 1996; Mingram et al., 2000; Yang et al., 2006).

The Cailing and Furong granites have distinct Sr–Nd isotopic compositions from the coeval mafic rocks (Fig. 13), and this rules out an origin of the Cailing and Furong granites by extensive fractional crystallization from coeval mafic magmas. Aluminous A-type granites have been interpreted as being generated by high-temperature partial melting of a felsic infracrustal source (King et al., 1997). However, this model might not be fully applicable to the Cailing and Furong granites. The granites almost are metaluminous. They also have relatively higher $\varepsilon_{Nd}(t)$ values, $\varepsilon_{Hf}(t)$ values and younger T_{DM} ages than Precambrian crusts and common S-type granites in Nanling Mountain (Fig. 13). Occurrence of MMEs in the granites and Sr–Nd–Hf isotopes indicate that the Qitianling granites might be derived from a well-homogenized, hybrid magma between anatexic granitic and mantle-derived mafic magmas. The Cailing and Furong granites have whole rock Nd isotopic model ages of 1.39 Ga to 1.56 Ga and zircon Hf isotopic model ages of 1.43 Ga to 1.71 Ga. Allowing for a ca. 20% decrease in the Sm/Nd ratio during melting and mixing with mafic magma, these Nd isotopic model ages increase to > 1.6 Ga, which suggests the Paleoproterozoic basement to be involved in partial melting at depth. Thus, the Cailing and Furong granites might be derived from anatexis of old crustal source induced by injection of mantle-derived magmas. This petrogenetic model can also be used to explain the reason for higher $\varepsilon_{Nd}(t)$ values and younger T_{DM} ages of granites in the Shi-Hang zone.

To further evaluate the mixing degree of the mantle-derived magma and crust-derived magma, we conduct an isotopic modeling of two end-member component mixing. The Ningyuan basalts were adopted as mantle component (Sr = 971 ppm, $^{87}Sr/^{86}Sr = 0.7035$, Nd = 37.6 ppm and $\varepsilon_{Nd}(t) = +5$, Li et al., 2004a) and the Precambrian crust as crustal component (Sr = 320 ppm, $^{87}Sr/^{86}Sr = 0.7180$, Nd = 27 ppm and $\varepsilon_{Nd}(t) = -10$). The mixing line is shown in Fig. 13. About 10%–20% mantle-derived magma fraction is necessary to generate the isotopic compositional range of the Cailing and Furong granites.

5.4. Tectonic environment

Recently, a series of high-precision zircon SHRIMP U–Pb age data have been reported on the granites in southern Hunan and northern Guangxi region in the Shi-Hang zone. These data provide important insight into understanding the genesis of this Mesozoic granite zone with higher ε_{Nd} (t) and younger T_{DM} ages. The Qianlishan granites yield zircon SHRIMP U–Pb ages of 152 ± 2 Ma (Li et al., 2004b). The Jinjiling and Xishan granites yield zircon SHRIMP U–Pb ages of about 156 Ma (Fu et al., 2004a,b; Jiang et al., 2009). The Huashan granites yield zircon SHRIMP U–Pb ages of 162 ± 1 Ma and the Guposhan granite yields ages of 163 ± 4 Ma (Zhu et al., 2006c). The emplacement ages of the Cailing and Furong granites are about 161 Ma and 156 Ma, respectively (Zhu et al., 2009). Considering the analytical error, all these data indicate that these granites with high $\varepsilon_{Nd}(t)$ values in southern Hunan and northern Guangxi region were emplaced in a narrow time interval of 152–163 Ma. These granites have similar geochemical characteristics and form a NNE-trending A-type granite belt (Jiang et al., 2008). All of them might be derived from curst–mantle magma mixing processes. Hence, these granites may have formed from the same continental extension event. From the southwest to the northeast, ages and $\varepsilon_{Nd}(t)$ values of the granites show a gradually decrease trend (Jiang et al., 2008). This indicates that the extension of the continental crust began from the southwest to the northeast, and the intensity of the extension decreased from the southwest to the northeast.

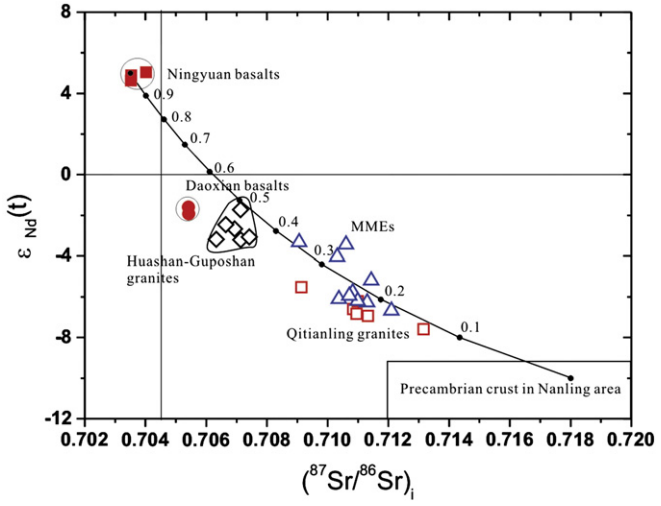

Fig. 13. Sr–Nd isotopic diagram of the Cailing and Furong granites and MMEs. Data of Ningyuan basalts and Daoxian basalts are from Li et al. (2004a).
Data of the Huashan–Guposhan granites are from Zhu et al. (2006a).

It has long been recognized that A-type magmas are formed in a variety of extensional regimes, from continental arc or back-arc extension to post-collisional extension and within-plate settings (e.g. Eby, 1992; Whalen et al., 1996; Förster et al., 1997). Eby (1992) suggested that the A_1 group seems to be restricted to hotspot, plume and continental rift zone located in anorogenic settings, whereas the A_2 group might be associated with the waning stages of arc magmatism. As mentioned above, the Qitianling granites belong to the A_2 group, thus an origin related to a hot spot, plume or continental rift zone located in anorogenic settings is unlikely.

The Indochina Block collided with the South China block along the Songma suture, and the peak age of the collision is dated at 258 Ma to 243 Ma (Carter et al., 2001). Then the South China Block collided with the North China Block along the Dabie-Sulu untrahigh-pressure metamorphic belt, and the peak age of the collision is dated at 240 Ma to 225 Ma (Li et al., 1993; Zheng, 2008). Thus, the South China Block was clamped between these two collision belts, resulting in a significant W-E trend compressional stress in the Indosinian era. In this period, strong folding, thrust faulting and nappe structure were developed in the South China Block (Shu et al., 1994; Zhang and Zhu, 2003; Liang et al., 2005; Zhang et al., 2011). The Indosinian granites in South China are dated at the cluster of 243–235 Ma and 218–210 Ma respectively, which were suggested to form as syn- and late-collisional granites (Zhou et al., 2006; Wang et al., 2007; Chen et al., 2011). Zhou et al. (2006) found that there was a ~25 Myr magmatically inactive period during the Early Jurassic (205–180 Ma) and suggested that this magmatic–tectonic quiescence in fact corresponds to the tectonic regime change from the Indosinian orogeny to the Yanshanian orogeny. The subduction of the paleo-Pacific plate underneath South China Block was suggested to start from the Early-Middle Jurassic (~180 Ma, Zhou et al., 2006; Jiang et al., 2009). The NNE trend of the Shi-Hang zone is completely different from the E-W trend of the Indosinian collision. We therefore suggest that the extensional event may have no relationship with the Indosinian collision.

There are some early Yanshanian (190–170 Ma) OIB-type basalts, gabbros and A-type granites occurring in southern Hunan, southern Jiangxi and southwestern Fujian provinces of South China (e.g. Chen et al., 1998; Zhao et al., 1998; Li et al., 2003; Xie et al., 2006; Wang et al., 2008). The small-scale early Jurassic magmatism is the incipience to long-term and large-scale Yanshanian magmatism in South China. They formed a near EW trend volcanic belt (Xie et al., 2006). Geochemical studies implied that these basalts were generated in within-plate tectonic setting and were suggested to be related to reactivation of the Indosinian near EW trend deep fault due to stress originated from the initial subduction of the paleo-Pacific plate from early Jurassic (Xie et al., 2006).

The Dexin granodiorite porphyry in the northeastern Jiangxi province was considered to be a part of the Shi-Hang zone in previous studies (Chen and Jahn, 1998; Wang et al., 2006). Recent studies indicated that the Dexin granodiorite porphyry was emplaced at about 171 Ma (Wang et al., 2006) and formed from arc magmatism (Zhou et al., 2011). The South China Block has suffered the subduction of the Izanagi ocean plate since Early to Middle Jurassic (Maruyama and Seno, 1986; Maruyama et al., 1997; Isozaki et al., 2010). Recent studies indicated that the farthest subduction of the paleo-Pacific plate may have reached the Shi-Hang zone (e.g. Jiang et al., 2009; Zhou et al., 2011). The paleo-Pacific plate did not subduct successively toward to the northwest. Instead slab roll-back occurred from the beginning of late Jurassic time (Jiang et al., 2009). Since the beginning of Late Jurassic time an intra-arc rift or a back arc basin has been formed along the Shi-Hang zone (Fig. 14; Jiang et al., 2006b, 2009). This setting is further supported by occurrence of the late Jurassic A_2-type Xiangshan volcanic complex and its low-Ti, high-Mg, potassic quenched enclaves within the North belt of the Shi-Hang zone (Jiang et al., 2005). Lithosphere extension, accompanying asthenosphere upwelling, may have triggered asthenosphere mantle to melt partially, and generate basaltic magma. Injection of these anomalously high temperature magmas into the granulitized lower crustal source region induced it to melt partially, generating the A-type magmas, such as the Cailing and Furong granites. Therefore, it is mostly likely that the southern Hunan and northern Guangxi region at the time of about 160 Ma is part of an intra-arc rift or back arc extensional zone induced by subduction of paleo-Pacific plate (Fig. 14). The strong mantle-derived and crust-derived magma mixing caused by the crustal extension generated the granites in this area.

6. Conclusions

The late Jurassic Cailing and Furong granites from the Qitianling batholith in the Shi-Hang zone belong to A-type and can be further classified to A_2-subtype. Zircon Hf isotopes of mafic enclaves and host granites provide direct evidence for mafic–felsic magma mixing processes. The mafic magma of MMEs might be originated from depleted mantle. The Cailing and Furong granites were derived from hybrid magma between old crust-derived felsic magma and mantle-derived mafic magma. The strong magma mixing caused by intra-arc rifting or back arc extension related to subduction of the paleo-Pacific plate, is favored to explain the petrogenesis of these granites.

Supplementary data associated with this article can be found, in the online version, at doi:10.1016/j.gr.2011.09.010.

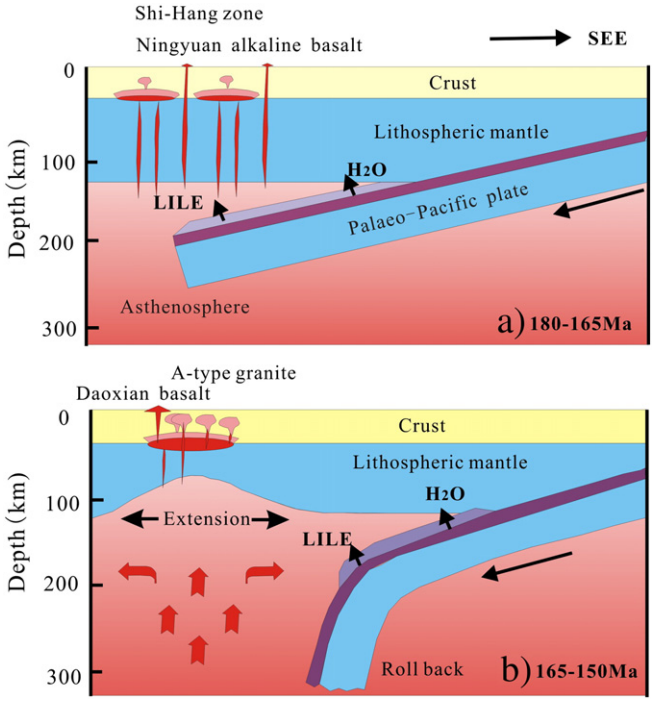

Fig. 14. Tectonic model for the generation and emplacement of the Qitianling granites (modified after Jiang et al., 2009). (a) The middle Jurassic mafic rocks were formed in a continental arc environment associated with subduction of the paleo-Pacific plate; (b)The Qitianling A-type granites were formed in a continental arc-rifting setting as a consequence of slab roll-back.

Acknowledgments

Dr. Lie-Wen Xie from the Institute of Geology and Geophysics, Chinese Academy of Sciences helped with zircon Hf isotope analyses. Comments and suggestions from Prof. Al Hofmann have improved this paper significantly. This work was supported by the National Nature Science Foundation of China grants (40603003, 40803006, 40873029), the Major State Basic Research Program of China (2012CB416706), and the Key Project of Chinese Ministry of Education (306007). We are grateful to Prof. M. Santosh, Prof. Zeming Zhang, Prof. Qiang Wang and two anonymous referees for constructive suggestions and criticisms in reviewing the manuscript.

References

Abdel-Rahman, A.M., 1994. Nature of biotites from alkaline, calc-alkaline, and peraluminous magmas. Journal of Petrology 35, 525–541.
Bai, D., Chen, J., Ma, T., Wang, X., 2005. Geochemical characteristics and tectonic setting of Qitianling A-type granitic pluton in southeast Hunan. Acta Petrologica et Mineralogica 24, 255–272 (in Chinese with English abstract).
Barbarin, B., 2005. Mafic magmatic enclaves and mafic rocks associated with some granitoids of the central Sierra Nevada batholith, California: nature, origin, and relations with the hosts. Lithos 80 (1–4), 155–177.
Blichert-Toft, J., Albarède, F., 1997. The Lu–Hf isotope geochemistry of chondrites and the evolution of the mantle–crust system. Earth and Planetary Science Letters 148 (1–2), 243–258.
Bonin, B., 2007. A-type granites and related rocks: evolution of a concept, problems and prospects. Lithos 97 (1–2), 1–29.
Boynton, W.L., 1984. Geochemistry of the rare earth elements: meteorite studies. In: Henderson, P. (Ed.), Rare earth element geochemistry. Elsevier, Amsterdam, pp. 63–114.
Carter, A., Roques, D., Bristow, C., Kinny, P., 2001. Understanding Mesozoic accretion in Southeast Asia: significance of Triassic thermotectonism (Indosinian orogeny) in Vietnam. Geology 29 (3), 211–214.
Chappell, B.W., White, A.J.R., 1974. Two constrasting granite types. Pacific Geology 8, 173–174.
Chappell, B.W., White, A.J.R., Wyborn, D., 1987. The importance of residual source material (restite) in granite petrogenesis. Journal of Petrology 28 (6), 1111–1138.
Chen, J., Jahn, B.M., 1998. Crustal evolution of southeastern China: Nd and Sr isotopic evidence. Tectonophysics 284 (1–2), 101–133.
Chen, P.R., Zhang, B.T., Kong, X.G., Cai, B.C., Ling, H.F., Ni, Q.S., 1998. Geochemical characteristics and tectonic implication of Zhaibei A-type granitic intrusive in South Jiangxi Province. Acta Petrologica Sinica 14 (3), 289–298 (in Chinese with English abstract).
Chen, C.H., Lee, C.Y., Shinjo, R., 2008. Was there Jurassic paleo-Pacific subduction in South China: constraints from $^{40}Ar/^{39}Ar$ dating, elemental and Sr–Nd–Pb isotope geochemistry of the Mesozoic basalts. Lithos 106, 83–92.
Chen, C.H., Hsieh, P.S., Lee, C.Y., Zhou, H.W., 2011. Two episodes of the Indosinian thermal event on the South China Block: constraints from LA-ICPMS U–Pb zircon and electron microprobe monazite ages of the Darongshan S-type granitic suite. Gondwana Research 19, 1008–1023.
Clemens, J.D., 2003. S-type granitic magmas—petrogenetic issues, models and evidence. Earth-Science Reviews 61 (1–2), 1–18.
Collins, W.J., Beams, S.D., White, A.J.R., Chappell, B.W., 1982. Nature and origin of A-type granites with particular reference to southeastern Australia. Contributions to Mineralogy and Petrology 80, 189–200.
Creaser, R.A., Price, R.C., Wormald, R.J., 1991. A-type granites revisited: assessment of a residual-source model. Geology 19 (2), 163–166.
Dahlquist, J.A., 2002. Mafic microgranular enclaves: early segregation from metaluminous magma (Sierra de Chepes), Pampean Ranges, NW Argentina. Journal of South American Earth Sciences 15 (6), 643–655.
Dai, B.Z., Jiang, S.Y., Jiang, Y.H., Zhao, K.D., Liu, D.Y., 2008. Geochronology, geochemistry and Hf–Sr–Nd isotopic compositions of Huziyan mafic xenoliths, southern Hunan Province, South China: petrogenesis and implications for lower crust evolution. Lithos 102 (1–2), 65–87.
Didier, J., Barbarin, B., 1991. Encalves and granite petrology, developments in petrology. Elsevier, Amsterdam. pp. 1–625.

Donaire, T., Pascual, E., Pin, C., Duthou, J.-L., 2005. Microgranular enclaves as evidence of rapid cooling in granitoid rocks: the case of the Los Pedroches granodiorite, Iberian Massif, Spain. Contributions to Mineralogy and Petrology 149 (3), 247–265.
Eby, G.N., 1990. The A-type granitoids: a review of their occurrence and chemical characteristics and speculations on their petrogenesis. Lithos 26 (1–2), 115–134.
Eby, G.N., 1992. Chemical subdivision of the A-type granitoids: petrogenetic and tectonic implications. Geology 20, 641–644.
Förster, H.J., Tischendorf, G., Trumbull, R.B., 1997. An evaluation of the Rb vs. (Y + Nb) discrimination diagram to infer tectonic setting of silicic igneous rocks. Lithos 40 (2–4), 261–293.
Fu, J.M., Ma, C.Q., Xie, C.F., Zhang, Y.M., Peng, S.B., 2004a. The determination of the formation age of the Xishan volcanic-intrusive complex in southern Hunan Province. Acta Geoscientica Sinica 25 (3), 303–308 (in Chinese with English abstract).
Fu, J.M., Ma, C.Q., Xie, C.F., Zhang, Y.M., Peng, S.B., 2004b. SHRIMP U–Pb zircon dating of the Jiuyishan composite granite in Hunan and its geological significance. Geotectonica et Metallogenia 28 (4), 370–378 (in Chinese with English abstract).
Fu, J.M., Ma, C.Q., Xie, C.F., Zhang, Y.M., Peng, S.B., 2004c. Zircon SHRIMP dating of the Cailing granite on the eastern margin of the Qitianling granite, Hunan, South China, and its significance. Geology in China 31, 96–100 (in Chinese with English abstract).
Fu, J.M., Ma, C.Q., Xie, C.F., Zhang, Y.M., Peng, S.B., 2005. Ascertainment of the Jinjiling aluminous A-type granite, Hunan Province, and its tectonic settings. Geochimica 34 (3), 215–226 (in Chinese with English abstract).
Gao, J.F., Lu, J.J., Lai, M.Y., Lin, Y.P., Pu, W., 2003. Analysis of trace elements in rock samples using HR-ICPMS. Journal of Nanjing University (Nature Sciences) 39, 844–850 (in Chinese with English abstract).
GERM, 2001. Geochemical Earth Reference Model. http://earthref.org/GERM/2001.
Gilder, S.A., Gill, J., Coe, R.S., Zhao, X.X., Liu, Z.W., Wang, G.X., 1996. Isotopic and paleomagnetic constraints on the Mesozoic tectonic evolution of South China. Journal of Geophysical Research 107 (B7), 16137–16154.
Giret, A., Bonin, B., Leger, J.M., 1980. Amphibole compositional trends in oversaturated and undersaturated alkaline plutonic ring-complexes. The Canadian Mineralogist 18, 481–495.
Griffin, W.L., Pearson, N.J., Belousova, E., Jackson, S.E., van Achterbergh, E., O''Reilly, S.Y., Shee, S.R., 2000. The Hf isotope composition of cratonic mantle: LAM-MC-ICPMS analysis of zircon megacrysts in kimberlites. Geochimica et Cosmochimica Acta 64 (1), 133–147.
Griffin, W.L., Wang, X., Jackson, S.E., Pearson, N.J., O'Reilly, S.Y., Xu, X., Zhou, X., 2002. Zircon chemistry and magma mixing, SE China: In-situ analysis of Hf isotopes, Tonglu and Pingtan igneous complexes. Lithos 61 (3–4), 237–269.
Guan, Q., Zhu, D.C., Zhao, Z.D., Dong, G.C., Zhang, L.L., Li, X.W., Liu, M., Mo, X.X., Liu, Y.S., Yuan, H.L., 2011. Crustal thickening prior to 38 Ma in southern Tibet: evidence from lower crust-derived adakitic magmatism in the Gangdese Batholith. Gondwana Research. doi:10.1016/j.gr.2011.07.004.
Hawkesworth, C.J., Kemp, A.I.S., 2006. Using hafnium and oxygen isotopes in zircons to unravel the record of crustal evolution. Chemical Geology 226 (3–4), 144–162.
Hawthorne, F.C., Oberti, R., 2007. Classification of the Amphiboles. Reviews in Mineralogy and Geochemistry 67, 55–88.
Hoskin, P.W.O., Schaltegger, U., 2003. The compositions of zircon and igneous and metamorphic petrogenesis. Reviews in Mineralogy and Geochemistry 53, 27–55.
Ishihara, S., 2007. Origin of the Cenozoic–Mesozoic magnetite-series and ilmenite-series granitoids in East Asia. Gondwana Research 11, 247–260.
Isozaki, Y., Aoki, K., Nakama, T., Yanai, S., 2010. New insight into a subduction-related orogeny: a reappraisal of the geotectonic framework and evolution of the Japanese Islands. Gondwana Research 18, 82–106.
Jiang, Y.H., Ling, H.F., Jiang, S.Y., Fan, H.H., Shen, W.Z., Ni, P., 2005. Petrogenesis of a Late Jurassic Peraluminous Volcanic Complex and its High-Mg, Potassic, Quenched Enclaves at Xiangshan, Southeast China. Journal of Petrology 46 (6), 1121–1154.
Jiang, S.Y., Zhao, K.D., Jiang, Y.H., Ling, H.F., Ni, P., 2006a. New type of tin mineralization related to granite in South China: evidence from mineral chemistry, element and isotope geochemistry. Acta Petrologica Sinica 22, 2509–2516 (in Chinese with English abstract).
Jiang, Y.H., Jiang, S.Y., Zhao, K.D., Ling, H.F., 2006b. Petrogenesis of Late Jurassic Qianlishan granites and mafic dykes, Southeast China: implications for a back-arc extension setting. Geological Magazine 143 (4), 457–474.
Jiang, S.Y., Zhao, K.D., Jiang, Y.H., Dai, B.Z., 2008. Characteristics and genesis of Mesozoic A-type granites and associated mineral deposits in the southern Hunan and northern Guangxi Provinces along the Shi-Hang belt, South China. Geological Journal of China University 14 (4), 496–509 (in Chinese with English abstract).
Jiang, Y.H., Jiang, S.Y., Dai, B.Z., Liao, S.Y., Zhao, K.D., Ling, H.F., 2009. Middle to late Jurassic felsic and mafic magmatism in southern Hunan province, southeast China: implications for a continental arc to rifting. Lithos 107 (3–4), 185–204.
Kerr, A., Fryer, B.J., 1993. Nd isotope evidence for crust-mantle interaction in the generation of A-type granitoid suites in Labrador, Canada. Chemical Geology 104 (1–4), 39–60.
King, P.L., White, A.J.R., Chappell, B.W., Allen, C.M., 1997. Characterization and Origin of Aluminous A-type Granites from the Lachlan Fold Belt, Southeastern Australia. Journal of Petrology 38 (3), 371–391.
King, P.L., Chappell, B.W., Allen, C.M., White, A.J.R., 2001. Are A-type granites the high-temperature felsic granites? Evidence from fractionated granites of the Wangrah Suite. Australian Journal of Earth Sciences 48 (4), 501–514.
Li, Z.X., Li, X.H., 2007. Formation of the 1300-km-wide intracontinental orogen and postorogenic magmatic province in Mesozoic South China: a flat-slab subduction model. Geology 35 (2), 179–182.
Li, S., Xiao, Y., Liou, D., Chen, Y., Ge, N., Zhang, Z., Sun, S.-S., Cong, B., Zhang, R., Hart, S.R., Wang, S., 1993. Collision of the North China and Yangtse Blocks and formation of coesite-bearing eclogites: timing and processes. Chemical Geology 109 (1–4), 89–111.
Li, X.H., Chen, Z.G., Liu, D.Y., Li, W.X., 2003. Jurassic gabbro–granite–syenite suites from Southern Jiangxi Province, SE China: Age, origin, and tectonic significance. International Geology Review 45, 898–921.
Li, X.H., Chung, S.L., Zhou, H.W., Lo, C.H., Liu, Y., Chen, C.H., 2004a. Jurassic intraplate magmatism in southern Hunan-eastern Guangxi: $^{40}Ar/^{39}Ar$ dating, geochemistry, Sr–Nd isotopes and implications for tectonic evolution of SE China. In: Malpas, J., Fletcher, C.J., Aitchison, J.C., Ali, J. (Eds.), Aspects of the Tectonic Evolution of China: Geological Society, London, Special Publications, 226, pp. 193–216.
Li, X.H., Liu, D., Sun, M., Li, W.X., Liang, X.R., Liu, Y., 2004b. Precise Sm–Nd and U–Pb isotopic dating of the supergiant Shizhuyuan polymetallic deposit and its host granite, SE China. Geological Magazine 141 (2), 225–231.
Li, X.H., Li, W.X., Li, Z.X., 2007a. On the genetic classification adn tectonic implications of the Early Yanshanian granitoids in the Nanling Range, South China. Chinese Science Bulletin 52, 1873–1885.
Li, X.H., Li, Z.X., Li, W.X., Liu, Y., Yuan, C., Wei, G., Qi, C., 2007b. U–Pb zircon, geochemical and Sr–Nd–Hf isotopic constraints on age and origin of Jurassic I- and A-type granites from central Guangdong, SE China: a major igneous event in response to foundering of a subducted flat-slab? Lithos 96 (1–2), 186–204.
Li, Z.L., Hu, R.Z., Yang, J.S., Peng, J.T., Li, X.M., Bi, X.W., 2007c. He, Pb and S isotopic constraints on the relationship between the A-type Qitianling granite and the Furong tin deposit, Hunan Province, China. Lithos 97 (1–2), 161–173.
Liang, X., Li, X., Qiu, Y., Yang, D., 2005. Indosinian collisional orogeny: evidence from structural and sedimentary geology in Shiwandashan Basin, South China. Geotectonica et Metallogenia 29, 99–112 (in Chinese with English abstract).
Litvinovsky, B.A., Jahn, B.M., Zanvilevich, A.N., Saunders, A., Poulain, S., Kuzmin, D.V., Reichow, M.K., Titov, A.V., 2002. Petrogenesis of syenite–granite suites from the Bryansky Complex (Transbaikalia, Russia): implications for the origin of A-type granitoid magmas. Chemical Geology 189 (1–2), 105–133.
Maas, R., Nicholls, I.A., Legg, C., 1997. Igneous and metamorphic enclaves in the S-type Deddick granodiorite, Lachlan Fold Belt, SE Australia: petrographic, geochemical and Nd–Sr isotopic evidence for crustal melting and magma mixing. Journal of Petrology 38 (7), 815–841.
Maruyama, S., Seno, T., 1986. Orogeny and relative plate motions: examples of the Japanese islands. Tectonophysics 127 (3–4), 305–329.
Maruyama, S., Isozaki, Y., Kimura, G., Terabayashi, M., 1997. Paleogeographic maps of the Japanese Islands: plate tectonic synthesis from 750 Ma to the present. The Island Arc 6 (1), 121–142.
Mingram, B., Trumbull, R.B., Littman, S., Gerstenberger, H., 2000. A petrogenetic study of anorogenic felsic magmatism in the Cretaceous Paresis ring complex, Namibia: evidence for mixing of crust and mantle-derived components. Lithos 54 (1–2), 1–22.
Mushkin, A., Navon, O., Halicz, L., Hartmann, G., Stein, M., 2003. The petrogenesis of A-type magmas from the Amram Massif, Southern Israel. Journal of Petrology 44 (5), 815–832.
Nowell, G.M., Kempton, P.D., Noble, S.R., Fitton, J.G., Saunders, A.D., Mahoney, J.J., Taylor, R.N., 1998. High precision Hf isotope measurements of MORB and OIB by thermal ionisation mass spectrometry: insights into the depleted mantle. Chemical Geology 149 (3–4), 211–233.
Perugini, D., Poli, G., Christofides, G., Eleftheriadis, G., 2003. Magma mixing in the Sithonia Plutonic Complex, Greece: evidence from mafic microgranular enclaves. Mineralogy and Petrology 78 (3), 173–200.
Pu, W., Zhao, K.D., Ling, H.F., Jiang, S.Y., 2004. High precision Nd isotope measurement by Triton TI mass spectrometry. Acta Geoscientica Sinica 25, 271–274 (in Chinese with English abstract).
Pu, W., Gao, J.F., Zhao, K.D., Ling, H.F., Jiang, S.Y., 2005. Seperation method of Rb–Sr, Sm–Nd using DCTA and HIBA. Journal of Nanjing University (Nature Sciences) 41, 445–450 (in Chinese with English abstract).
Scherer, E., Munker, C., Mezger, K., 2001. Calibration of the Lutetium–Hafnium clock. Science 293 (5530), 683–687.
Shu, L., Guo, L., Shi, Y., Sun, Y., 1994. Kinematic study on the southern marginal fault zone of the Jiuling Mountains, Jiangxi Province. Scientia Geologica Sinica 29, 209–219 (in Chinese with English abstract).
Sparks, R.S.J., Marshall, L., 1986. Thermal and mechanical constraints on mixing between mafic and silicic magmas. Journal of Volcanology and Geothermal Research 29, 99–124.
Streckeisen, A., Le Maitre, R.W., 1979. A chemical approxination to the modal QAPF classification of the igneous rocks. Neues Jahrbuch fur Mineralogie Abteilung 136, 169–206.
Sun, S.S., McDonough, W.F., 1989. Chemical and isotopic systematics of oceanic basalt: implication for mantle composition and processes. In: Saunders, A.D., Norry, M.J. (Eds.), Magmatism in the Ocean Basins: Geological Society, London, Specical Publications, 42, pp. 529–548.
Tanaka, T., Togashi, S., Kamioka, H., Amakawa, H., Kagami, H., Hamamoto, T., Yuhara, M., Orihashi, Y., Yoneda, S., Shimizu, H., Kunimaru, T., Takahashi, K., Yanagi, T., Nakano, T., Fujimaki, H., Shinjo, R., Asahara, Y., Tanimizu, M., Dragusanu, C., 2000. JNdi-1: a neodymium isotopic reference in consistency with LaJolla neodymium. Chemical Geology 168 (3–4), 279–281.
Turner, S.P., Foden, J.D., Morrison, R.S., 1992. Derivation of some A-type magmas by fractionation of basaltic magma: an example from the Padthaway Ridge, South Australia. Lithos 28 (2), 151–179.
Vernon, R.H., 1984. Microgranitoid enclaves in granites: globules of hybrid magma quenched in a plutonic environment. Nature 309, 438–439.
Vernon, R.H., Etheridge, M.A., Wall, V.J., 1988. Shape and microstructure of microgranitoid enclaves: Indicators of magma mingling and flow. Lithos 22 (1), 1–11.
Wang, X., Griffin, W.L., O'Reilly, S.Y., Zhou, X.M., Xu, X.S., Jackson, S.E., Pearson, N.J., 2002. Morphology and geochemistry of zircons from late Mesozoic igneous

complexes in coastal SE China: implications for petrogenesis. Mineralogical Magazine 66 (2), 235–251.
Wang, R.C., Fontan, F., Chen, X.M., Hu, H., Liu, C.S., Xu, S.J., de Parseval, P., 2003a. Accessory minerals in the Xihuashan Y-enriched granitic complex, southern china: a record of magmatic and hydrothermal stages of evolution. The Canadian Mineralogist 41, 727–748.
Wang, X., Griffin, W.L., Wang, Z., Zhou, X.M., 2003b. Hf isotope compositions of zircons and implications for the petrogenesis of Yajiangqiao granite, Hunan Province, China. Chinese Science Bulletin 48, 995–998.
Wang, Y.J., Fan, W.M., Guo, F., 2003c. Geochemistry of early Mesozoic potassium-rich diorite–granodiorites in southeastern Hunan Province, South China: petrogenesis and tectonic implications. Geochemical Journal 37, 427–448.
Wang, Q., Xu, J.F., Jian, P., Bao, Z.W., Zhao, Z.H., Li, C.F., Xiong, X.L., Ma, J.L., 2006. Petrogenesis of adakitic porphyries in an extensional tectonic setting, Dexing, South China: implication for the genesis of porphyry copper mineralization. Journal of Petrology 47, 119–144.
Wang, Y.J., Fan, W.M., Sun, M., Liang, X.Q., Zhang, Y.H., Peng, T.P., 2007. Geochronological, geochemical and geothermal constraints on petrogenesis of the Indosinian peraluminous granites in the South China Block: a case study in the Hunan Province. Lithos 96 (3–4), 475–502.
Wang, Y.J., Fan, W.M., Cawood, P.A., Li, S., 2008. Sr–Nd–Pb isotopic constraints on multiple mantle domains for Mesozoic mafic rocks beneath the South China Block hinterland. Lithos 106, 297–308.
Watson, E.B., Harrison, T.M., 1983. Zircon saturation revisited: temperature and composition effects in a variety of crustal magma types. Earth and Planetary Science Letters 64, 295–304.
Whalen, J.B., Currie, K.L., Chappell, B.W., 1987. A-type granites: geochemical characteristics, discrimination and petrogenesis. Contributions to Mineralogy and Petrology 95 (4), 407–419.
Whalen, J.B., Jenner, G.A., Longstaffe, F.J., Robert, F., Gariépy, C., 1996. Geochemical and Isotopic (O, Nd, Pb and Sr) Constraints on A-type granite petrogenesis based on the Topsails igneous suite, Newfoundland Appalachians. Journal of Petrology 37 (6), 1463–1489.
White, A.J.R., Chappell, B.W., Wyborn, D., 1999. Application of the restite model to the Deddick granodiorite and its enclaves —a reinterpretation of the observations and data of Maas et al. (1997). Journal of Petrology 40 (3), 413–421.
Wickham, S.M., Alberts, A.D., Zanvilevich, A.N., Litvinovsky, B.A., Bindeman, I.N., Schauble, E.A., 1996. A stable isotope study of anorogenic magmatism in east central Asia. Journal of Petrology 37 (5), 1063–1095.
Wong, J., Sun, M., Xing, G.F., Li, X.H., Zhao, G.C., Wong, K., Wu, F.Y., 2011. Zircon U–Pb and Hf isotopic study of Mesozoic felsic rocks from eastern Zhejiang, South China: geochemical contrast between the Yangtze and Cathaysia blocks. Gondwana Research 19, 244–259.
Wu, Y.B., Zheng, Y.F., 2004. Genesis of zircon and its constraints on interpretation of U–Pb age. Chinese Science Bulletin 49 (15), 1554–1569.
Wu, F.Y., Jahn, B.M., Wilde, S.A., Lo, C.H., Yui, T.F., Lin, Q., Ge, W.C., Sun, D.Y., 2003. Highly fractionated I-type granites in NE China (I): geochronology and petrogenesis. Lithos 66 (3–4), 241–273.
Wu, F.Y., Yang, Y.H., Xie, L.W., Yang, J.H., Xu, P., 2006. Hf isotopic compositions of the standard zircons and baddeleyites used in U–Pb geochronology. Chemical Geology 234, 105–126.
Xie, X., Xu, X.S., Zhou, H.B., Jiang, S.Y., Zhang, M., Qiu, J.S., 2006. Early J2 basalts in SE China: incipience of large-scale late Mesozoic magmatism. Science in China, Series D: Earth Sciences 49 (8), 796–815.
Xu, P., Wu, F.Y., Xie, L.W., 2004. Hf isotopic compositions of the standard zircons for U–Pb dating. Chinese Science Bulletin 49, 1642–1648.
Yang, C., Zhu, J.C., Zhang, P.H., Xie, C.F., 2005. Geochemical characteristics and genesis of dioritic enclaves in Lisong granites, NE Guangxi Province. Geological Journal of China University 12 (3), 310–318 (in Chinese with English abstract).
Yang, J.H., Wu, F.Y., Chung, S.L., Wilde, S.A., Chu, M.F., 2006. A hybrid origin for the Qianshan A-type granite, northeast China: geochemical and Sr–Nd–Hf isotopic evidence. Lithos 89 (1–2), 89–106.
Yang, J.H., Wu, F.Y., Wilde, S.A., Xie, L.W., Yang, Y.H., Liu, X.M., 2007. Tracing magma mixing in granite genesis: in-situ U–Pb dating and Hf isotope analysis of zircons. Contributions to Mineralogy and Petrology 153 (2), 177–190.
Zen, E., 1988. Phase relationships of peraluminous granitic rocks and their petrogenetic implications. Annual Review of Earth and Planetary Sciences 16, 21–51.
Zhang, K.J., Zhu, J.X., 2003. Intracontinental deformation of South China due to penetration of North China: fold and thrust structures and their ore-controlling in southern Anhui, South China. Journal of Nanjing University (Nature Sciences) 39, 746–753 (in Chinese with English abstract).
Zhang, F.F., Wang, J.Y., Chen, X.Y., Fan, W.M., Zhang, Y.H., Zhang, G.W., Zhang, A.M., 2011. Triassic high-strain shear zones in Hainan Island (South China) and their implications on the amalgamation of the Indochina and South China Blocks: kinematic and $^{40}Ar/^{39}Ar$ geochronological constraints. Gondwana Research 19, 910–925.
Zhao, Z.H., Bao, Z.W., Zhang, B.Y., 1998. Geochemistry of the Mesozoic basaltic rocks in southern Hunan Province. Science in China, Series D: Earth Sciences 4, 102–112 (Supp.).
Zhao, Z.H., Bao, Z.W., Zhang, B.Y., Xiong, X.L., 2001. Crust–mantle interaction and its contribution to the Shizhuyuan tungsten-polymetallic mineralization. Science in China, Series D: Earth Sciences 44 (3), 266–276.
Zhao, K.D., Jiang, S.Y., Jiang, Y.H., 2005a. Geological and geochemistry of the Furong tin deposit, Hunan Province. In: Mao, J.W., Bierlein, F.P. (Eds.), Mineral Deposit Research: meeting the global challenge. Springer, pp. 869–871.
Zhao, K.D., Jiang, S.Y., Jiang, Y.H., Wang, R.C., 2005b. Mineral chemistry of the Qitianling granitoid and the Furong tin ore deposit in Hunan Province, South China: implication for the genesis of granite and related tin mineralization. European Journal of Mineralogy 17, 635–648.
Zhao, K.D., Jiang, S.Y., Jiang, Y.H., Liu, D.Y., 2006. SHRIMP U–Pb dating of the Furong unit of Qitianling granite from southeast Hunan Province and their geological implications. Acta Petrologica Sinica 22 (10), 2611–2616 (in Chinese with English abstract).
Zhao, K.D., Jiang, S.Y., Zhu, J.C., Li, L., Dai, B.Z., Jiang, Y.H., Ling, H.F., 2010. Hf isotopic composition of zircons from the Huashan–Guposhan intrusive complex and mafic enclaves in northeastern Guangxi: implication for petrogenesis. Chinese Science Bulletin 55, 509–519.
Zheng, Y.-F., 2008. A perspective view on ultrahigh-pressure metamorphism and continental collision in the Dabie-Sulu orogenic belt. Chinese Science Bulletin 53 (20), 3081–3104.
Zheng, J.J., Jia, B.H., 2001. Geological characteristics and related tin-polymetallic mineralization of the Qitianling granite complex in southern Hunan Province. Geology and Mineral Resources of South China 4, 50–57 (in Chinese with English abstract).
Zhou, X.M., Li, W.X., 2000. Origin of Late Mesozoic igneous rocks in Southeastern China: implications for lithosphere subduction and underplating of mafic magmas. Tectonophysics 326 (3–4), 269–287.
Zhou, X.M., Sun, T., Shen, W.Z., Shu, L.S., Niu, Y.L., 2006. Petrogenesis of Mesozoic granitoids and volcanic rocks in South China: a response to tectonic evolution. Episodes 29 (1), 26–33.
Zhou, Q., Jiang, Y.H., Zhao, P., Liao, S.Y., Jin, G.D., 2011. Origin of the Dexing Cu-bearing porphyries, SE China: elemental and Sr-Nd-Pb-Hf isotopic constraints. International Geology Review. doi:10.1080/00206814.2010.548119.
Zhu, J.C., Huang, G.F., Zhang, P.H., 2003. On the emplacement age and material sources for the granites of Cailing superunit, Qitianling pluton, South Hunan Province. Geological Review 49 (3), 245–252 (in Chinese with English abstract).
Zhu, J.C., Xie, C.F., Zhang, P.H., Yang, C., Gu, C., 2005. Niumiao and Tong'an intrusive bodies of NE Guangxi: petrology, zircon SHRIMP U–Pb geochronology and geochemistry. Acta Petrologica Sinica 21 (3), 665–676 (in Chinese with English abstract).
Zhu, J.C., Zhang, P.-H., Xie, C.-F., Zhang, H., Yang, C., 2006a. The Huashan–Guposhan A-type granitoid belt in the western part of the Nanling Mountains: petrology, geochemistry, and genetic interpretation. Acta Geologica Sinica 80 (4), 529–542 (in Chinese with English abstract).
Zhu, J.C., Zhang, P.H., Xie, C.F., Zhang, H., Yang, C., 2006b. Magma mixing origin of the mafic enclaves in Lisong granite, NE Guangxi, western Nanling Mountains. Geochimica 35 (5), 506–516 (in Chinese with English abstract).
Zhu, J.C., Zhang, P.H., Xie, C.-F., Zhang, H., Yang, C., 2006c. Zircon U–Pb age framework of Huashan–Guposhan intrusive belt, western part of Nanling Range, and its geological significance. Acta Petrologica Sinica 22 (9), 2270–2278 (in Chinese with English abstract).
Zhu, J.C., Chen, J., Wang, R.C., Lu, J.J., Xie, L., 2008. Early Yanshanian NE trending Sn/W-bearing A-type granites in the western-middle part of the Nanling Mts region. Geological Journal of China Universities 14, 474–484 (in Chinese with English abstract).
Zhu, J.C., Wang, R.C., Zhang, P.H., Xie, C.F., Zhang, W.L., Zhao, K.D., Xie, L., Yang, C., Che, X.D., Yu, A.P., Wang, L.B., 2009. Zircon U–Pb geochronological framework of Qitianling granite batholiths, middle part of Nanling Range, South China. Science in China, Series D: Earth Sciences 52 (9), 1279–1294.